



Supplementary Materials for

Myofibroblast proliferation and heterogeneity is supported by macrophages during skin repair

Brett A. Shook, Renee R. Wasko, Guillermo C. Rivera Gonzalez, Emilio Salazar-Gatzimas, Francesc López-Giráldez, Biraja C. Dash, Andrés R. Muñoz-Rojas, Krystal D. Aultman, Rachel K. Zwick, Vivian Lei, Jack L. Arbiser, Kathryn Miller-Jensen, Damon A. Clark, Henry C. Hsia, Valerie Horsley

correspondence to: brett.shook@yale.edu; valerie.horsley@yale.edu

This PDF file includes:

Materials and Methods
Figs. S1 to S21
Table S1 to S3
References 78-88

Materials and Methods:

Mice and Animal Procedures

All animal care and experiments followed guidelines issued by Yale University's Institutional Animal Care and Use Committee (IACUC). C57/Bl6 mice were purchased from Charles River. Aged mice (>24 months old) were obtained from the NIA. Previously described *Pdgfra* H2B:GFP (Stock #007669), *LysMCre* (Stock #004781) and iDTR mice (Stock #007900) were purchase from Jackson Laboratories. *En1Cre;Rosa26*-LSL-tdTomato mice were received from the laboratory of R. Atit (Case Western Reserve University, Cleveland, OH) by crossing *Engrailed 1*-Cre mice (Jackson Laboratories Stock #007196) with *Rosa26*-LSL-tdTomato mice (Jackson Laboratories Stock #007914). *Mgl2*^{DTR/GFP} mice were developed by the laboratory of A. Iwasaki (Yale University, New Haven, CT) (46). *PdgfraCreER* mice were developed in the laboratory of B. Hogan (Duke University, Durham, NC)(68) and *Dlk1CreER* (*Pref1CreER*) mice were developed in the laboratory of C. Wolfrum (ETH Zürich, Schwerzenbach, Switzerland)(69). For lineage-tracing experiments, *PdgfraCreER* and *Dlk1CreER* mice were crossed with *Rosa26mT/mG* mice (Jackson Laboratories Stock #007676). 7-9 week-old male mice were wounded during the telogen phase of hair cycling. Mice were anesthetized using isofluorane and four or six full-thickness wounds, 3-4mm apart, were made on shaved back skin using a 4mm biopsy punch (Accuderm). Bleomycin-mediated fibrosis was induced in 7-9 week old C57/Bl6 mice injected subcutaneously with bleomycin (10mg/kg/day) (Enzo Life Sciences) or PBS for 5 days as previously reported (13). For EdU experiments, 50mg/kg of EdU (Invitrogen) was injected intraperitoneally at indicated time points and detected per manufacturer protocols. To genetically deplete

myeloid cells, *LysMCre;iDTR* mice were given 50 μ l of 20 μ g/ml diphtheria toxin (DT) (Sigma) in PBS via tail vein injection. To deplete CD301b-expressing cells, 25 μ l of 20 μ g/ml DT was administered intraperitoneally to *Mgl2^{DTR/GFP}* mice. The number of newly generated monocyte-derived myeloid cells were reduced by orally administering 80mg/kg of the cFMS inhibitor GW2580 (Cayman) every 12 hours as previously described (70, 71). Tamoxifen (5mg/mL in ethanol; 50 μ l for neonatal and 100 μ l for adult mice, Sigma Aldrich) was topically administered to shaved dorsal skin of resulting *Dlk1CreER;mT/mG* and *PdgfraCreER;mT/mG* mice (fig. S7).

Fluorescence activated cell sorting and analysis - mouse

Mouse back skin and wound beds were dissected and digested into single cells using 1:100 collagenase 1A (Worthington) for adipocyte precursor cells or Liberase TM for macrophage subsets, as previously described (26, 41, 72). Cells were resuspended in FACS staining buffer (1% BSA in PBS with 2mM EDTA). To examine immune cell subsets, cells were stained with the following antibodies for 30 minutes on ice: CD45-PE-Cy7 (eBioscience, 1:2000), CD11b-Alexa700 (eBioscience, 1:500), F4/80-eFluor450 (eBioscience, 1:50), CD206-Alexa488 (Biolegend, 1:500), MHC-II-eFluor450 (eBioscience, 1:1000), CD64-PerCp (Biolegend, 1:500) and CD301b-Alexa660 (eBioscience, 1:100). Wound macrophages were defined as CD45⁺;CD11b⁺;F4/80⁺ cells. To examine mesenchymal heterogeneity, cells were stained with the following antibodies for 20 minutes on ice: CD45-APC-eFluor780 (eBioscience, 1:2000), CD31-APC-Fire750 (Biolegend, 1:1000), CD29-Alexa700 (eBioscience, 1:400), CD34-Pacific Blue (BD Bioscience, 1:50), Sca1-V500, -FITC or -PE (eBioscience, 1:500), CD26-PE-Cy7 (Biolegend, 1:500), CD9-APC (BD Bioscience, 1:100), CD9-FITC (eBioscience, 1:100)

and CD90 (1:250, Biolegend). APs were identified based on cell surface markers as previously described (CD45⁻, CD31⁻, CD29⁺, CD34⁺ and Sca1⁺) (26, 28, 72, 73). Intracellular flow cytometry using α SMA-FITC (eBioscience, 1:500) and Collagen 1 (Abcam, 1:250) was performed as previously described (26). Analysis of proliferation using EdU incorporation was performed using the Click-iT EdU Flow Cytometry Assay Kit per the manufacturer's instructions. To exclude dead cells, Sytox Orange or Sytox Blue (Invitrogen, 1:1000) was added immediately before sorting using a FACS Aria III with FACS DiVA software (BD Biosciences). Cells were sorted into 10% fetal bovine serum (FBS) in DMEM and flow cytometry analysis was performed using FlowJo Software (FlowJo).

Fluorescence activated cell sorting and analysis - human

Freshly collected human skin tissue samples discarded from surgical procedures were obtained in accordance with Yale IRB guidelines and transported to the lab in sterile PBS for immediate processing. Briefly, skin samples were sterilized in 10% betadine (2 min), then twice in 70% ethanol (1 min) followed by sterile PBS for 1 min. The tissue samples were then transferred to 100mm cell culture petri dishes and most of the adipose tissue was removed using a scalpel prior to mincing. Minced tissue was incubated in 15 mL of enzymatic dissociation solution, containing 0.25% of Trypsin-EDTA; 1mg/mL of dispase and collagenase I and II for 90 minutes at 37°C. Digested tissue was vortexed and pipetted vigorously, then passed through a 70 μ m filter. Enzyme inactivation was performed in 10% FBS containing DMEM medium and the cell pellet was resuspended in 5% BSA solution and incubated at room temperature for 30 min. 1x10⁶ cells/100 μ l were then incubated with the following fluorophore-attached primary antibodies for 45

minutes at room temperature: CD45-Pacific Blue (Biolegend 1:100), CD31-Pacific Blue (Biolegend, 1:100), CD90-PE-Cy7 (BD Bioscience, 1:20), CD34-APC (eBioscience, 1:20), CD29-APC-Cy7 (Biolegend, 1:20), CD26-PE (BD Bioscience, 1:5) and CD9-FITC (eBioscience, 1:20). Cells were washed twice with PBS, then resuspended in 500µL of FACS buffer (0.1% BSA in PBS) and analyzed on a BD LSRII. Compensation for all the fluorophores was performed using commercially available compensation beads (Cat A10513; ThermoFisher) and was applied to the final analysis. Flow cytometry analysis was performed using FlowJo Software (FlowJo).

RNA extraction and Real-Time PCR

For naïve and wound bed APs and wound bed immune cells, FACS-purified samples were digested using TRIzol LS (Invitrogen), RNA was extracted from the aqueous phase using the RNeasy Plus Micro Kit (Qiagen). cDNA was generated using equal amounts of total RNA with the Superscript III First Strand Synthesis Kit (Invitrogen) per manufacturer instructions. Total RNA was obtained from low input mesenchymal subsets using the Absolutely RNA Nanoprep Kit (Agilent). All quantitative real-time PCR was performed using SYBR green on a LightCycler 480 (Roche). Primers for specific genes are listed in Supplementary Table 3. Results were normalized to β -actin as previously described (72). Data show representative technical replicates. Similar trends were observed in 3 biological samples.

RNA-sequencing

Quality RNA samples were selected (RIN>7) and RNA-seq was performed as previously described (74). For APs and immune cells, single-end 50bp RNA-seq was performed using an Illumina HiSeq 2000 sequencer at the Yale Stem Cell Center for Genome

Analysis. Low input RNA processing was conducted on individual mesenchymal subsets. From each cellular subset, 500pg-1ng of total RNA was purified and converted to cDNA using the SMARTer Ultra Low V4 RNA kit (Clonetech) per manufacturer protocols. Samples were sequenced using 76 bp single-end sequencing on an Illumina HiSeq 2500 according to Illumina protocols at the Yale Center for Genomic Analysis. The first nucleotide and the last nucleotides with a quality score below 20 for each read were trimmed using in-house scripts. If, after trimming, the read was shorter than 45-bp, the whole read was discarded. Trimmed reads were aligned with TopHat v.2.1.1 to the reference UCSC mouse genome and transcript annotation (mm10). Only the reads that mapped to a single unique location within the genome, with a maximum of two mismatches in the anchor region of the spliced alignment, were reported in these results. TopHat alignments were then processed by Cufflinks v2.2.1 to identify differentially expressed genes (75). Significantly differentially expressed genes (experimental logarithmic (log₂) ratio >1, FDR-adjusted p<0.05) were analyzed using Ingenuity Pathway Analysis software suite (Qiagen) as previously described (26).

Fibroblast Functional Assays

Hydroxyproline content To analyze collagen production, mesenchymal cell subsets were sorted into phenol red-free DMEM (Gibco) containing 10% FBS, then processed for hydroxyproline content as previously described (76). Briefly, cells were homogenized and incubated in hydrochloric acid overnight at 120°C, then processed per manufacturer protocols (Sigma Aldrich) and the absorbance at 560nm was measured using a SpectraMax 250 plate reader (Molecular Devices). Hydroxyproline content was

calculated using a standard curve and normalized to the number of cells sorted for each sample.

Collagen crosslinking lox assay FACS-isolated cells (4×10^4 /mL) were cultured overnight and conditioned media was processed to test the ability of mesenchymal cells to crosslink collagen. The Amplate Fluorimetric Lysyl Oxidase Assay Kit (AAT Bioquest) was performed per the manufacturer's protocol and imaged using a SpectraMax Gemini EM plate reader (Molecular Devices).

Fibroblast migration assay Wound beds were dissected from back skin, bisected and cultured in 10% FBS in DMEM (ATCC) in chamber slides (ThermoFisher) for 3 days. Fibroblast migration was quantified by measuring the distance between the final cell position and the wound bed edge.

Cell Transplants

FACS-purified cell populations were counted using a hemocytometer and diluted in FACS staining buffer at a concentration of 3.0×10^6 cells/ml. 10 μ l of cell suspension (~30,000 cells) was slowly injected into wound beds of anesthetized congenic littermates using a 30G needle.

In vitro AP proliferation and differentiation

FACS-isolated APs were cultured as described previously (26, 28). Cells were sorted and plated on carboxyl-coated 24-well plates (BD Biosciences, 354775) in DMEM supplemented with 10% FBS. At 50% confluence, APs were switched to 0.5% FBS DMEM overnight then treated with 5 μ m EdU for 16 hours in combination with 15,000 cells added onto a Transwell mesh insert (Corning) or recombinant proteins (CCL6, CCL8, CXCL4, IGF1 or PDGFCC (Peprotech)). EdU was detected per manufacturer's protocol (Invitrogen). Adipogenic potential was examined by allowing APs to grow to

confluence and subsequently treated with DMEM supplemented with 10% FBS and MDI cocktail (30 μ g/ml IBMX, 0.25 μ g/ml dexamethasone and 1 μ g/ml insulin) (Sigma-Aldrich) for 2 days. Cultured APS were then treated with fresh DMEM supplemented with 10% FBS and insulin (1 μ g/ml) every 2 days for 6 additional days and lipid content was quantified using standard Oil Red O staining, as previously described (27).

Neutralizing antibodies and pharmacological signaling pathway inhibitors

To inhibit signaling pathways *in vivo*, mice were injected intraperitoneally with the PDGFR α inhibitor Crenolanib (Caymen, 20mg/kg), the IGF1R inhibitor Linsitinib (Caymen, 50mg/kg) or the PI3K inhibitor Wortmannin (Caymen, 1mg/kg). To block ligand binding, mice received local injections, 5 μ g per wound, of neutralizing antibodies against PDGFC or IGF1 (R&D Systems), as previously described (77).

Immunofluorescence and wound bed analysis

Mouse wound beds were embedded in O.C.T. and sectioned through their entirety to identify the center of the wound bed. 14 μ m cryosections were processed as previously described (41) and stained with the following antibodies: Collagen I (1:500, Abcam), CD26 (1:250, Abcam or 1:50, Novus Biologicals), CD29 (1:50, Novus Biologicals), CD31 (rat, 1:100; BD Biosciences), CD34 (1:100, eBioscience), CD45 (1:500, eBioscience), CD301b (1:100, R&D Systems), ER-TR7 (rat, 1:500; Abcam), Itga6 (1:300, R&D Systems) and SMA (1:500, Abcam). Histological quantification for each wound bed was conducted on the three central-most sections, and the averages from two wounds were averaged for each animal. Re-epithelialization and corrected total fluorescence were calculated using ImageJ software (National Institutes of Health,

Bethesda, MD) as described previously (73, 78). Revascularization was calculated using Adobe Photoshop to measure the total CD31⁺ pixels divided by the total number of pixels in wound beds. To determine spatial localization of myofibroblast subsets and CD301b⁺ macrophages, sections from the center of wound beds were immunostained and imaged in their entirety. The wound bed was bisected down the midline and analyzed using MATLAB to determine the signal intensity of individual channels throughout the superficial to deep and medial to lateral axes. Keloids were obtained from de-identified patients from the Emory University Department of Pathology. The tissue was embedded in paraffin per routine histology processing and 4 μ m sections were collected. Following antigen retrieval in sodium citrate, samples were stained with CD301 (1:25, R&D Systems).

Measurement of cytokine secretion

Cells from wound beds were sorted as described above, and plated at a density of 150,000 cells per well in 12-well plates. Cell culture medium was collected after a 12-hour incubation and assayed by ELISA according to the manufacturer's recommendations (R&D, IGF-I cat. #: DY791, CCL3 cat. #: DY450, CCL8 cat. #: DY790). Briefly, microwell plates were coated with capture antibody overnight and then blocked for 1 hour with PBS + 1% BSA. A recombinant protein standard curve and the sample cell culture medium were then incubated in the coated wells for 2 hours, followed by incubation with biotinylated detection antibody for 2 hours. Finally, the wells were incubated with horseradish peroxidase (HRP) conjugated to streptavidin for 20 minutes, and then with a colorimetric substrate solution for 20 minutes. The reaction was stopped and the absorbance measured in a spectrophotometer. The concentration of the samples

was interpolated from a standard curve and statistical significance was determined using a two-tailed unpaired t-test.

Statistics

To determine significance between two groups, comparisons were made using Student's *t*-test. Analyses across multiple groups were made using a one-way ANOVA with Bonferroni's *post hoc* using GraphPad Prism for Mac (GraphPad Software, La Jolla, CA) with significance set at $p<0.05$.

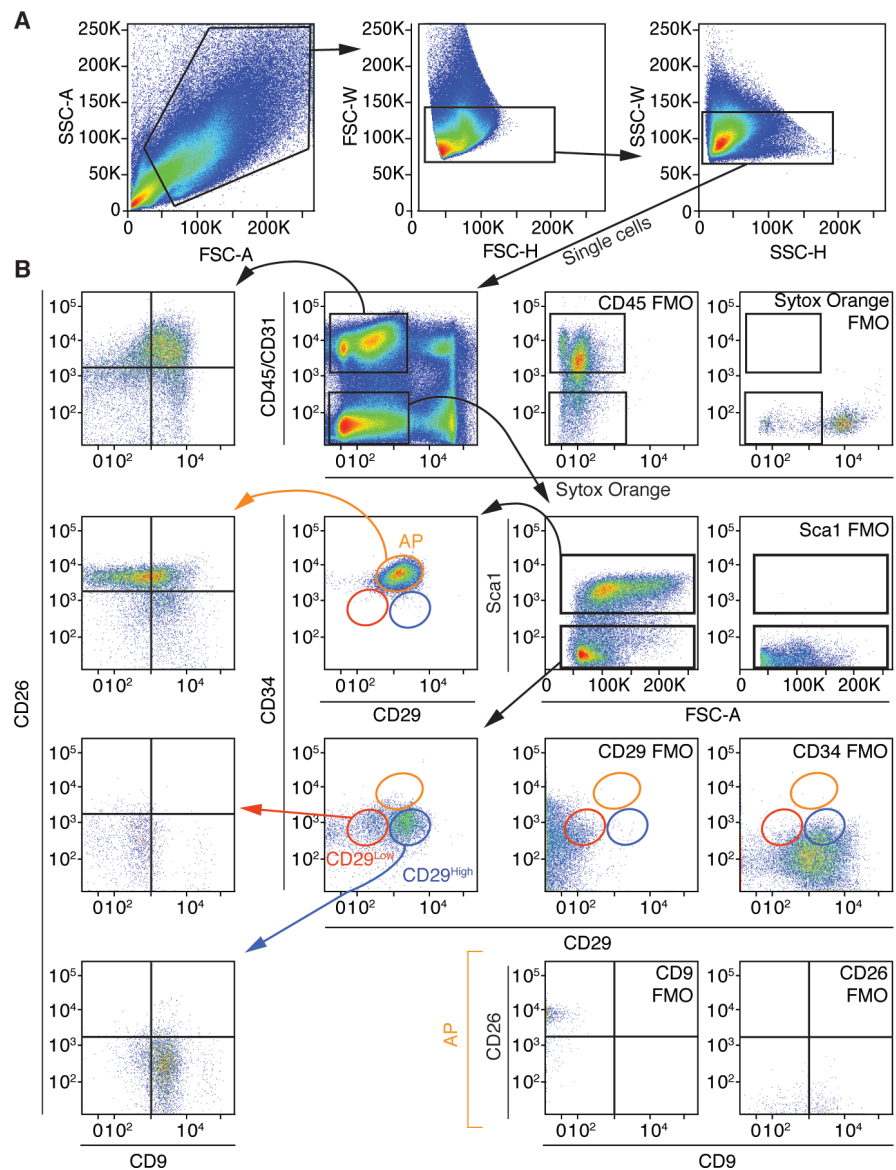


Fig. S1. Characterization of mesenchymal cell surface marker heterogeneity. (A) FACS plots and gating strategy for single cell identification. (B) Gating strategy and fluorescence minus one (FMO) FACS plots used to examine mesenchymal cell heterogeneity.

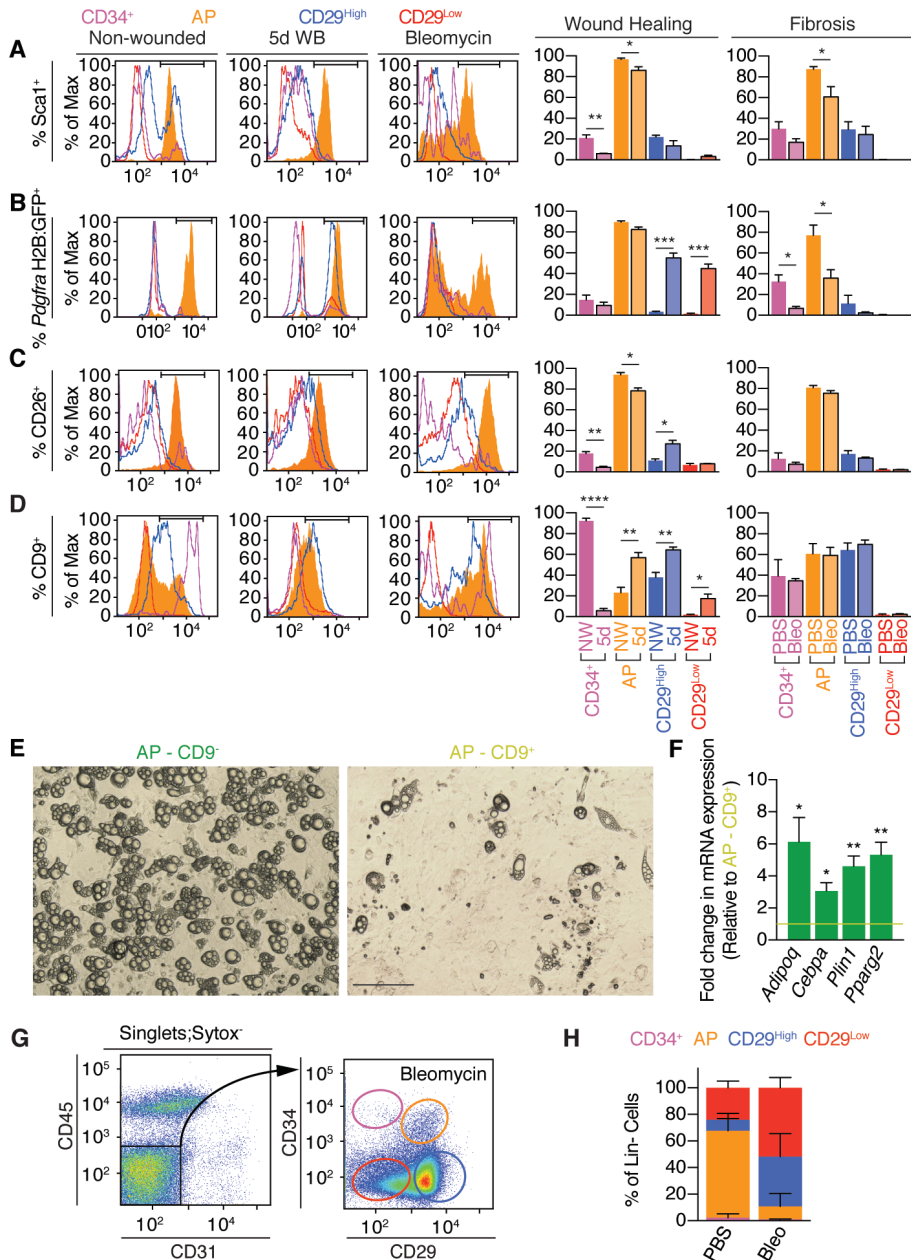


Fig. S2. Characterization of profibrotic mesenchymal cell heterogeneity. (A to D)

Flow cytometry histograms (left) and quantification (right) showing colocalization of CD34 and CD29 subpopulations with Sca1 (A), *Pdgfra*-GFP (B), CD26 (C) and CD9 (D) after injury or bleomycin-induced fibrosis ($n \geq 3$). (E) Bright field images of adipocytes differentiated from CD9⁺ and CD9⁻ AP subsets isolated from non-wounded skin. Scale bar, 100 μ m. (F) Gene expression comparison of AP subsets following adipogenic induction ($n = 4$). (G) FACS plots of CD29 and CD34 mesenchymal cells in skin treated with bleomycin for 5 days. (H) Quantification of cellular subsets in bleomycin-induced fibrosis (PBS, $n = 4$; bleomycin (bleo), $n = 3$). All error bars indicate mean \pm SEM. * $p < 0.05$, ** $p < 0.01$, *** $p < 0.001$, **** $p < 0.0001$.

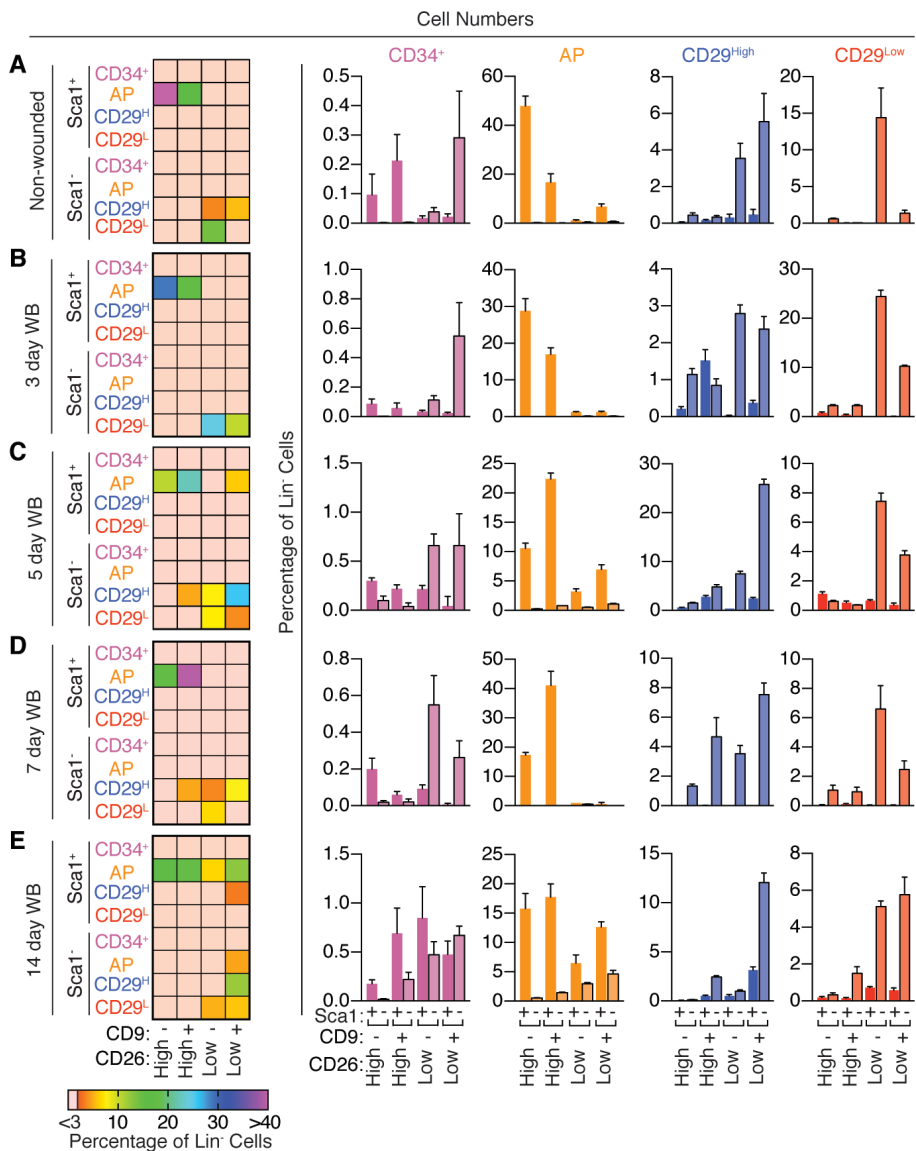


Fig. S3. Mesenchymal cell heterogeneity continuously changes during tissue repair. (A to E) Heat maps (left) and bar graphs (right) quantification of mesenchymal subset in non-wounded ($n = 11$) (A), 3-day ($n = 4$) (B), 5-day ($n = 6$) (C), 7-day ($n = 4$) (D) and 14-day ($n = 13$) (E) wound beds (WB). All error bars indicate mean \pm SEM.

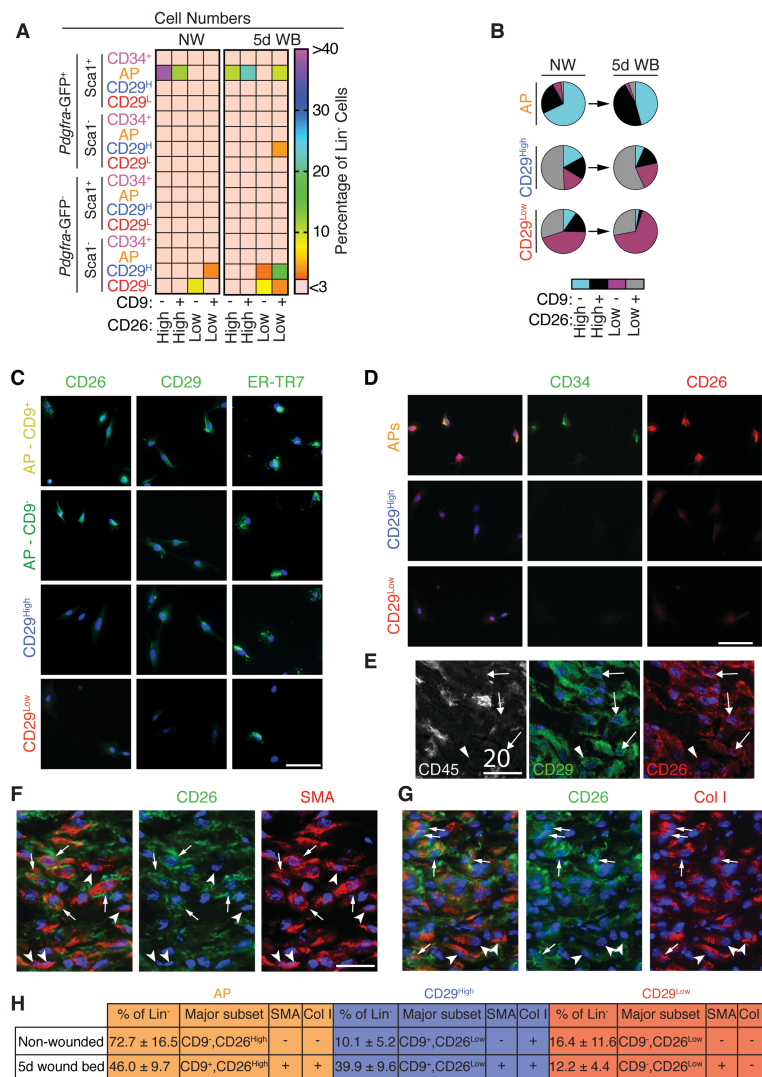


Fig. S4. Characterization of the fibrotic phenotype in wound bed mesenchymal cells.

(A) Heat map of lineage negative mesenchymal cells ($n = 6$). (B) Pie charts depicting changes in relative abundance of CD9 and CD26 colocalization on the most abundant mesenchymal subsets in non-wounded and 5-day wound beds ($n = 6$). (C and D) Immunofluorescent staining of FACS-isolated cell populations for fibroblast markers. APs are CD26^{High} and CD29^{High} and CD29^{Low} cells are CD26^{Low}. Scale bar, 50µm. (E to G) Images from 5-day wound beds showing SMA (F) and Collagen I (G) colocalization with APs (CD45⁻;CD29⁺;CD26^{High}) and CD26^{Low} cells. Arrows indicate CD26^{High} cells and arrowheads indicate CD26^{Low} cells. Scale bars, 20µm. (H) Table summarizing changes that occur in colocalization with pro-fibrotic molecular markers in adipocyte precursor (AP), CD29^{High} and CD29^{Low} cell pools during wound healing ($n = 6$).

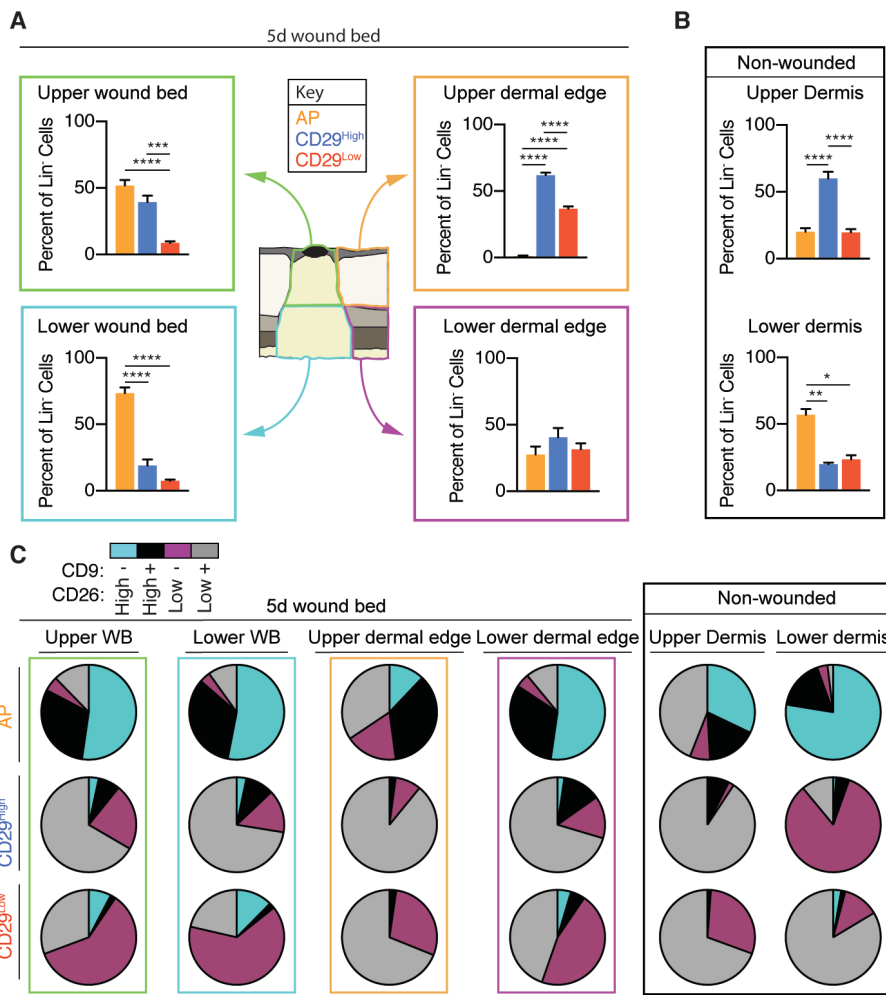


Fig. S5. Myofibroblast are spatially biased in skin wound beds. (A to C) Wound beds were dissected into distinct regions prior to processing for flow cytometry. Quantification of the relative abundance of mesenchymal cell subsets based on location in 5-day wound beds ($n = 5$) (A) and non-wounded skin ($n = 4$) (B). (C) CD9 and CD26 colocalization on each cellular subset based on spatial location in wound beds and non-wounded skin. All error bars indicate mean \pm SEM. * $p < 0.05$, ** $p < 0.01$, *** $p < 0.001$, **** $p < 0.0001$.

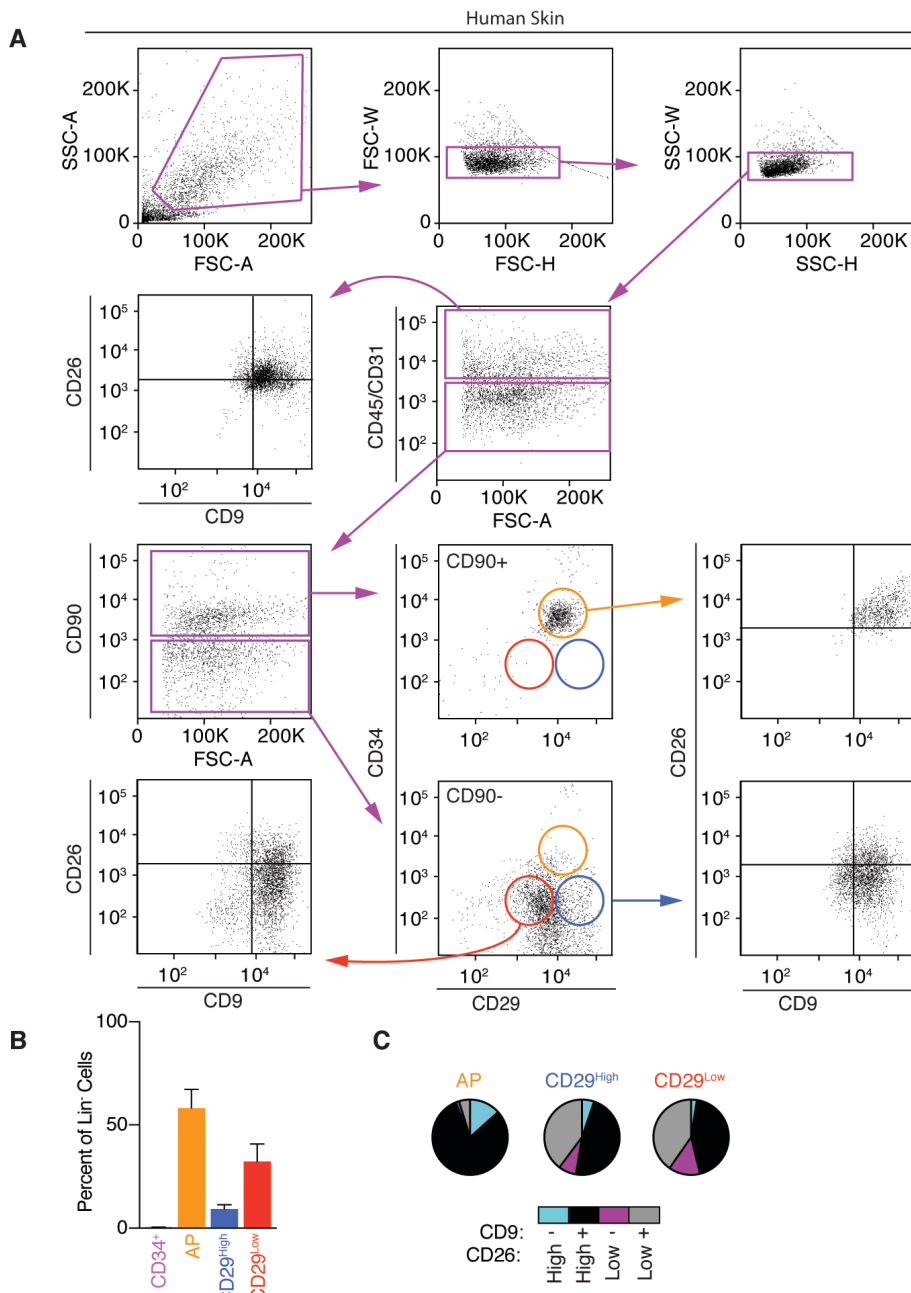


Fig. S6. Human skin mesenchymal cells are enriched with pro-fibrotic markers. (A) FACS plots and gating strategy used to delineate mesenchymal cell populations in non-wounded human skin. **(B)** Quantification of Lin⁻ mesenchymal subsets and **(C)** CD9 and CD26 colocalization within each subpopulation.

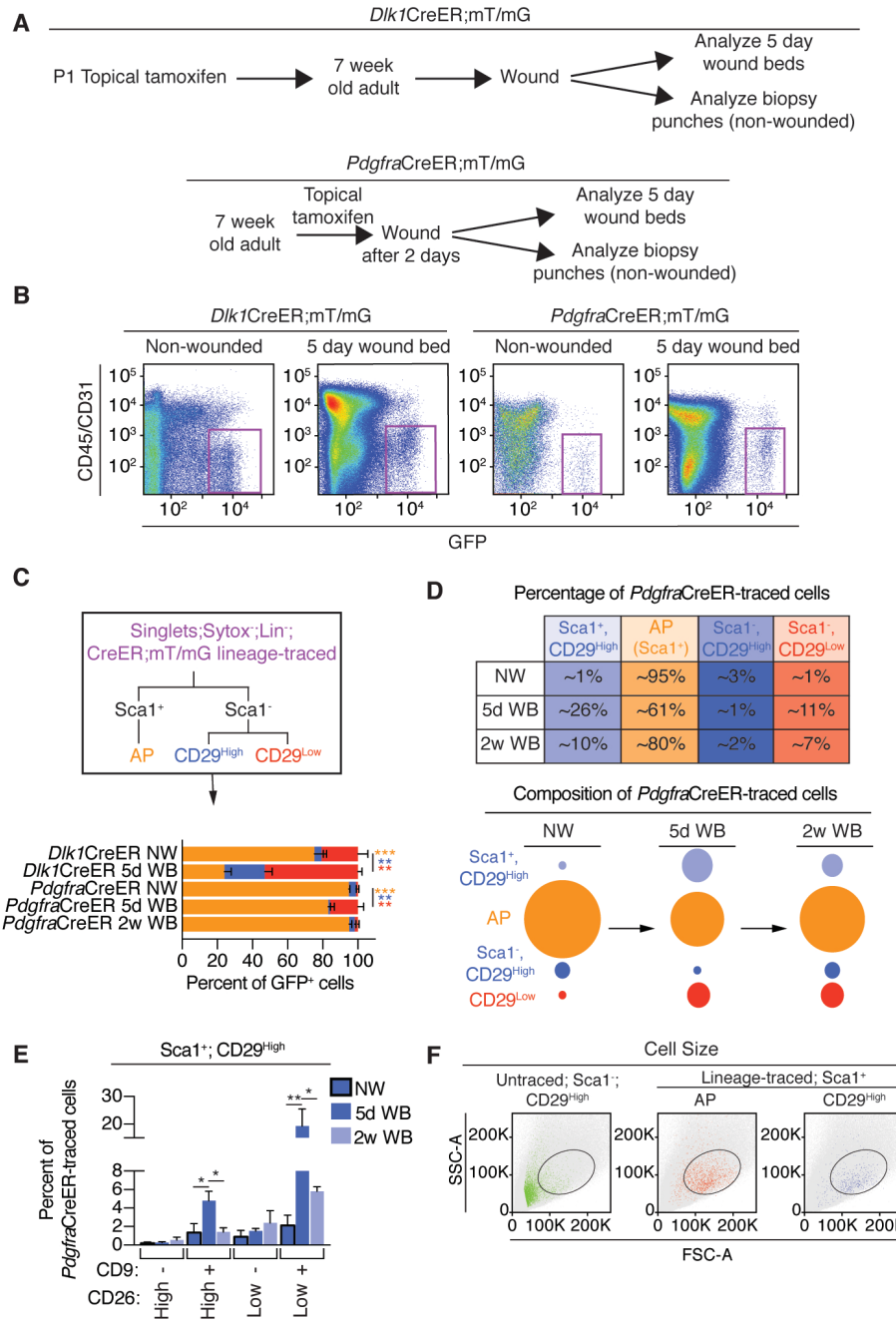


Fig. S7. Genetic lineage tracing of wound bed fibroblasts. (A) Induction strategy for lineage tracing wound bed fibroblasts. (B) Flow plot of single cells analyzed for lineage tracing. (C) Relative abundance of APs, CD29^{High} and CD29^{Low} lineage traced cells in *Dlk1CreER* ($n = 4$) and *PdgfraCreER* ($n = 4$) mouse lines. (D) Quantification and schematic of lineage-traced wound bed fibroblasts reveal robust expansion of populations that are infrequent in non-wounded skin, including Sca1⁺;CD29^{High} cells. Circle size reflects relative abundance of cellular population. (E) Quantification of CD26 and CD9 colocalization of Sca1⁺;CD29^{High} lineage traced cells. (F) Flow plots of FSC-A and SSC-A reveal similar cellular properties between APs and Sca1⁺;CD29^{High} cells. All error bars indicate mean \pm SEM. * $p < 0.05$, ** $p < 0.01$, *** $p < 0.001$.

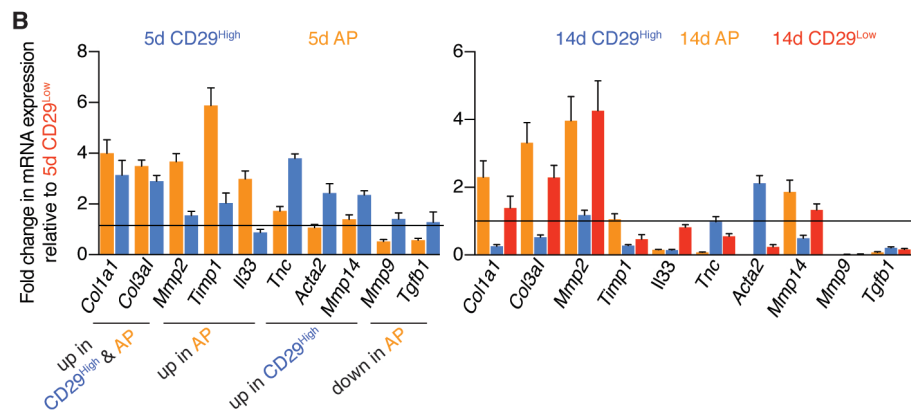
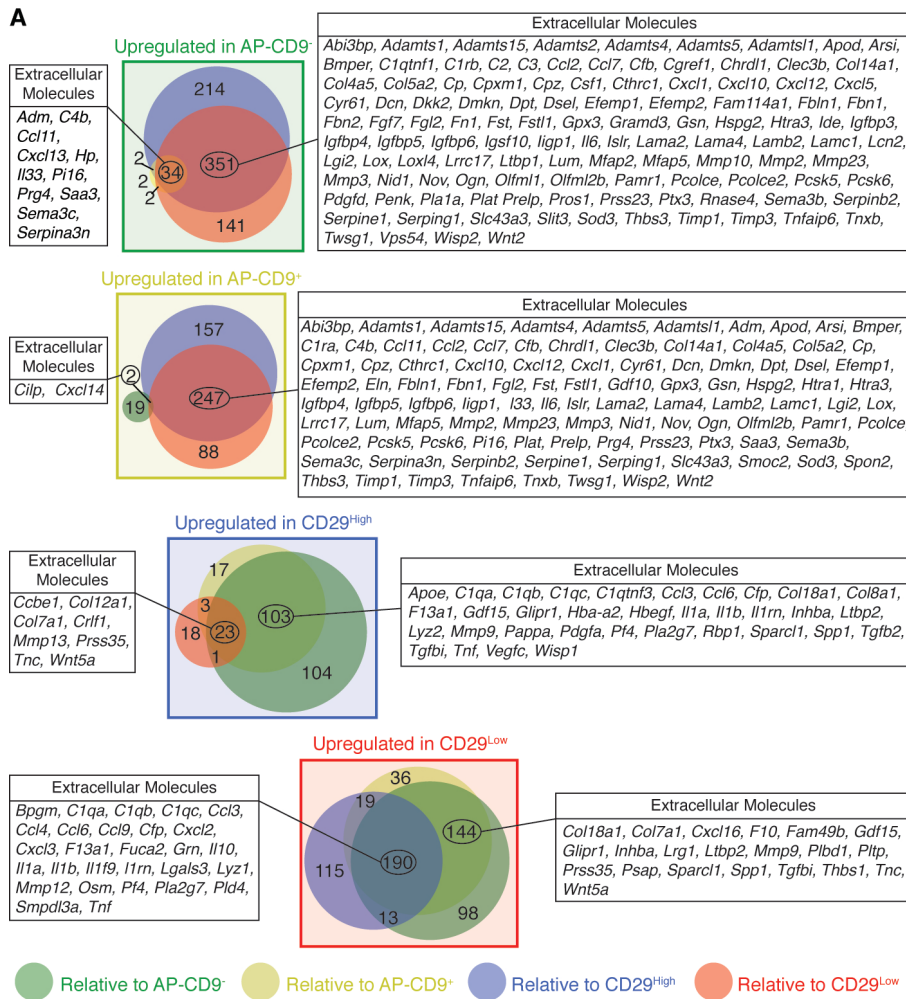


Fig. S8. Myofibroblast subsets have unique gene expression profiles. (A) Venn diagrams of genes upregulated in individual cell populations. Tables list extracellular molecules that are differentially expressed relative to other subsets. (B) Gene expression in 5-day and 14-day wound bed myofibroblast subsets of genes differentially expressed in RNA-sequencing analysis. Black lines indicate expression levels in 5-day CD29^{Low} cells. All error bars indicate mean ± SEM.

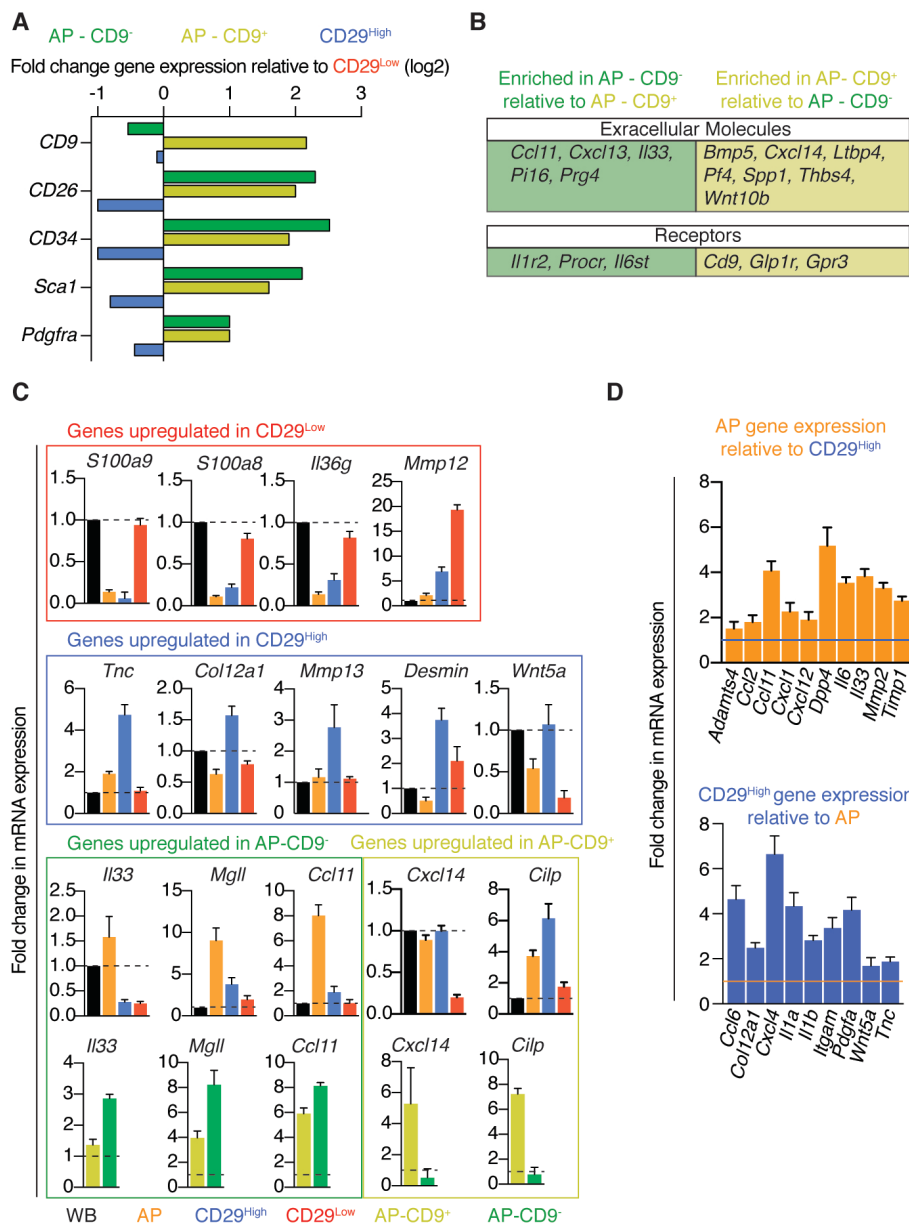


Fig. S9. Gene expression analysis of myofibroblast subsets from 5-day wound beds.

(A) Bar graph of gene enrichment for molecular markers used to distinguish myofibroblast subsets compared to expression in CD29^{Low} cells. Values are taken from RNA-sequencing results. **(B)** Genes differentially expressed between CD9⁻ and CD9⁺ AP populations. **(C)** Real-time qPCR analysis of genes differentially expressed in RNA-seq. Black bars and dotted lines indicates expression level in total wound bed. **(D)** Real-time qPCR analysis of genes differentially expressed between APs and CD29^{High} cells, revealed by RNA-seq. All error bars indicate mean \pm SEM.

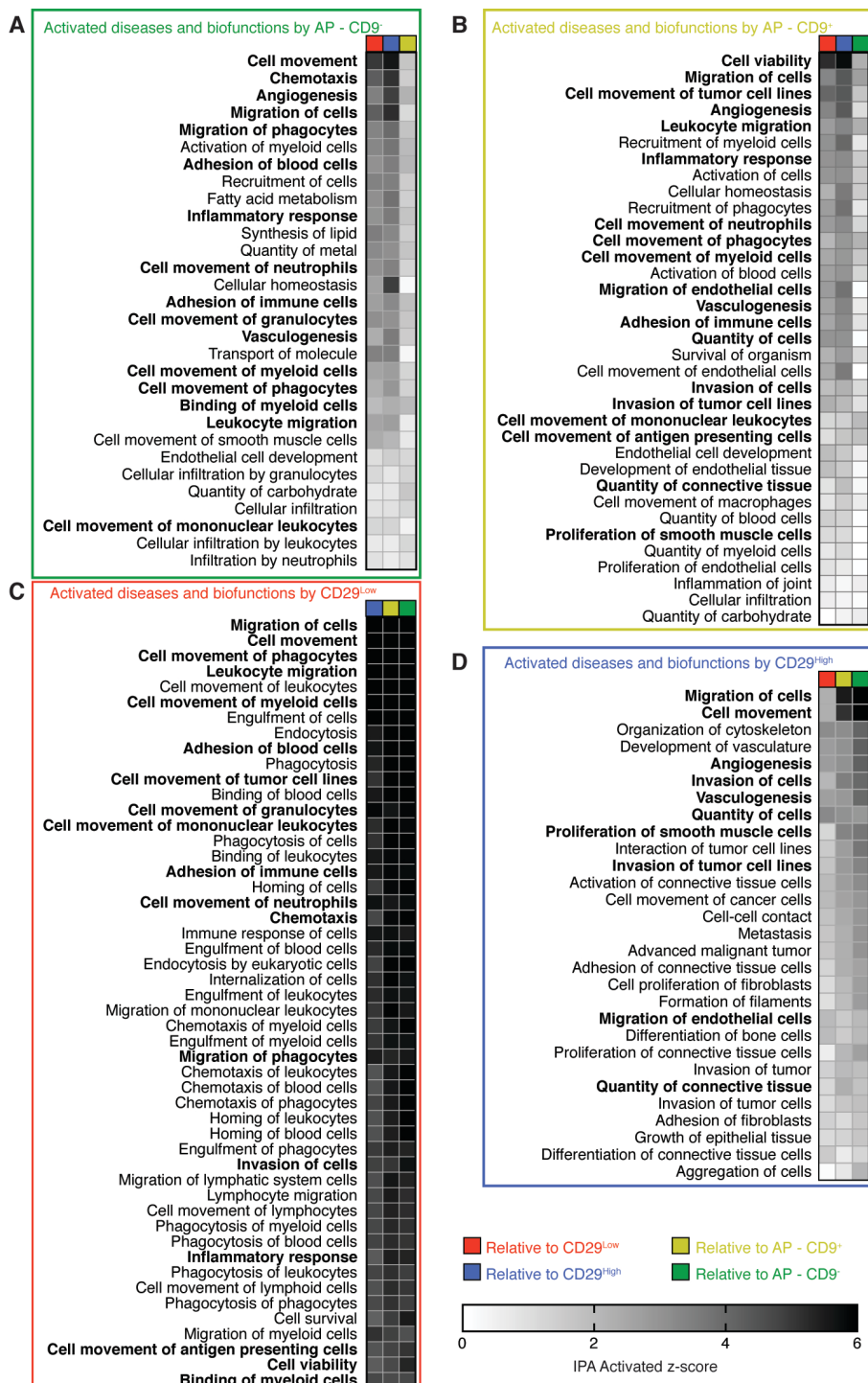


Fig. S10. Predicted biofunctions activated by individual mesenchymal cell subsets. (A to D) IPA analysis of upregulated gene profiles predicted the top biofunctions that can be activated by individual mesenchymal cell populations. Biofunctions in bold text were predicted to be activated by an AP subset (A and B) and a non-AP subset (C and D), showing overlapping functions based on unique gene expression profiles.

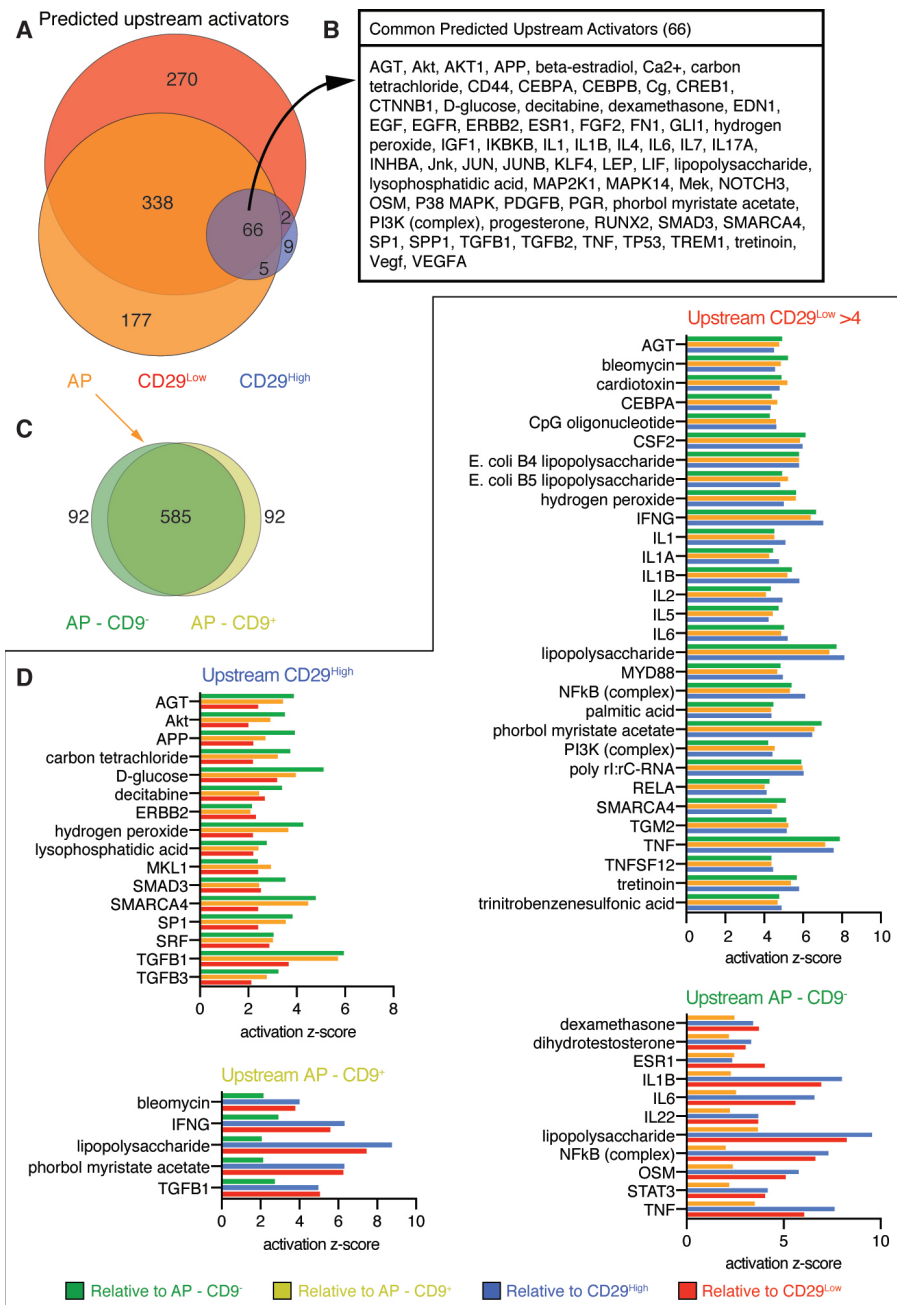


Fig. S11. Predicted upstream activators of unique mesenchymal cell gene expression profiles. IPA analysis predicted upstream activators that could lead to upregulated genes in individual mesenchymal cell populations. **(A)** Venn diagram (A) and list of common upstream activators (B). **(C)** Venn diagram of upstream activators of each AP subset. **(D)** Graphs of z-scores from the top IPA predicted upstream activators of upregulated gene expression profiles between individual cell populations.

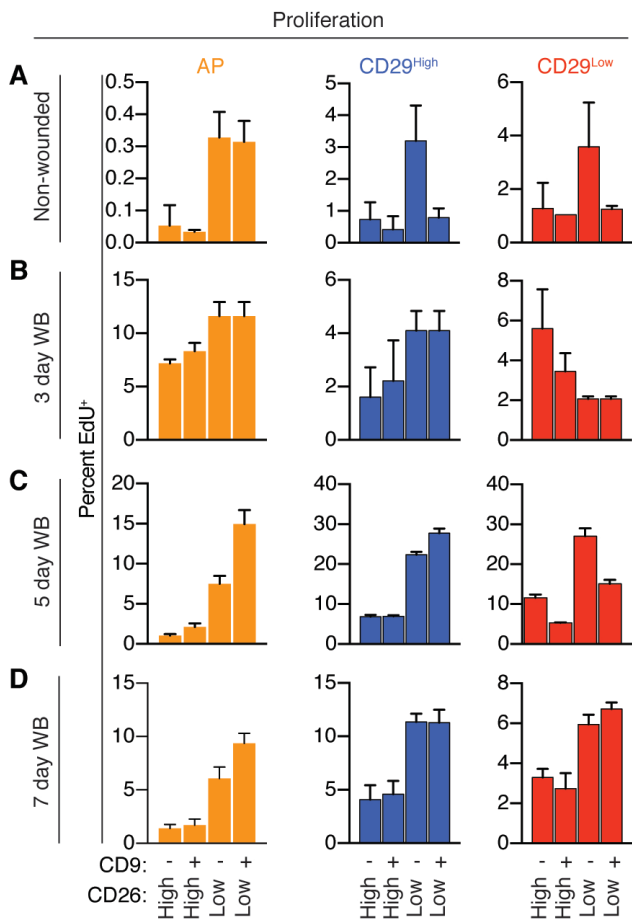


Fig. S12. Proliferation rates of mesenchymal cell subsets are heterogeneous and change during tissue repair. (A to D) Quantification of EdU incorporation in mesenchymal subsets in non-wounded ($n = 4$) (A), 3-day ($n = 4$) (B), 5-day ($n = 4$) (C) and 7-day ($n = 4$) (D) wound beds (WB). Mice were given EdU 4 hours prior to sacrificing. All error bars indicate mean \pm SEM.

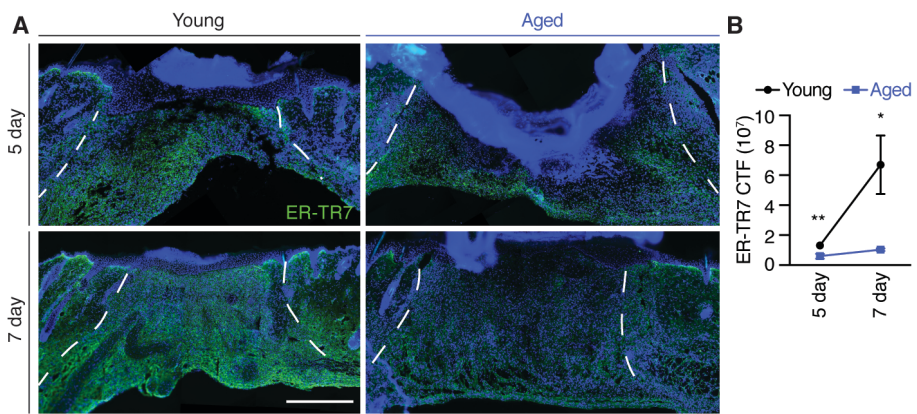


Fig. S13. Fibroblast repopulation is delayed during aging. (A) Representative images of fibroblast ER-TR7 antibody staining in day 5 and 7 wound beds of young (7 week old) and aged (>24 month old) mice. White lines delineate wound edges. Scale bar, 750 μ m. (B) Quantification of ER-TR7 Corrected Total Fluorescence (CTF) in young and aged wound beds. 5-day ($n = 4$, $p = 0.0086$), 7-day ($n = 4$, $p = 0.0180$). All error bars indicate mean \pm SEM.

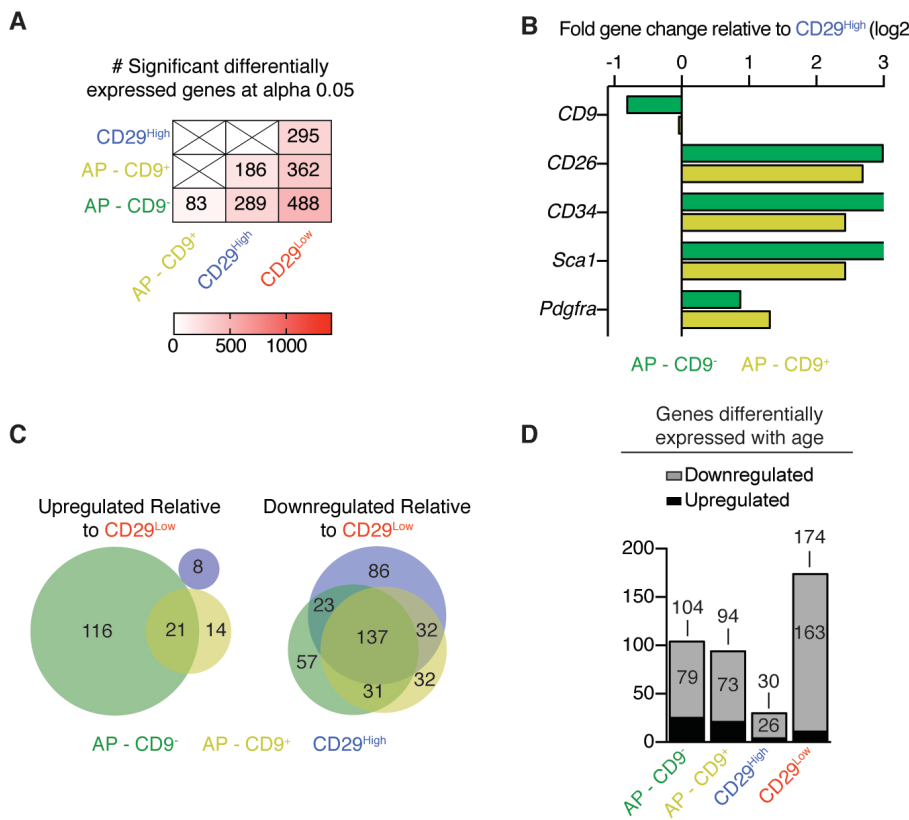


Fig. S14. Differential gene expression is not robustly activated in wound bed myofibroblasts from aged mice. RNA-sequencing was performed on subsets of 5-day wound bed myofibroblasts from aged mice. **(A)** Heat map of genes differentially expressed between myofibroblast populations in 5-day wound beds from aged mice. **(B)** Bar graph of gene enrichment for molecular markers used to distinguish APs compared to expression in CD29^{High} cells. Values are taken from RNA-sequencing results. **(C)** Venn diagram of genes upregulated and downregulated in aged myofibroblast populations relative to CD29^{Low} cells. Overlap represents enriched genes present in multiple cellular populations. **(D)** Quantification of differentially expressed genes in young versus aged myofibroblast subsets. Numbers indicate the total number of differentially expressed genes and the number of genes downregulated with age.

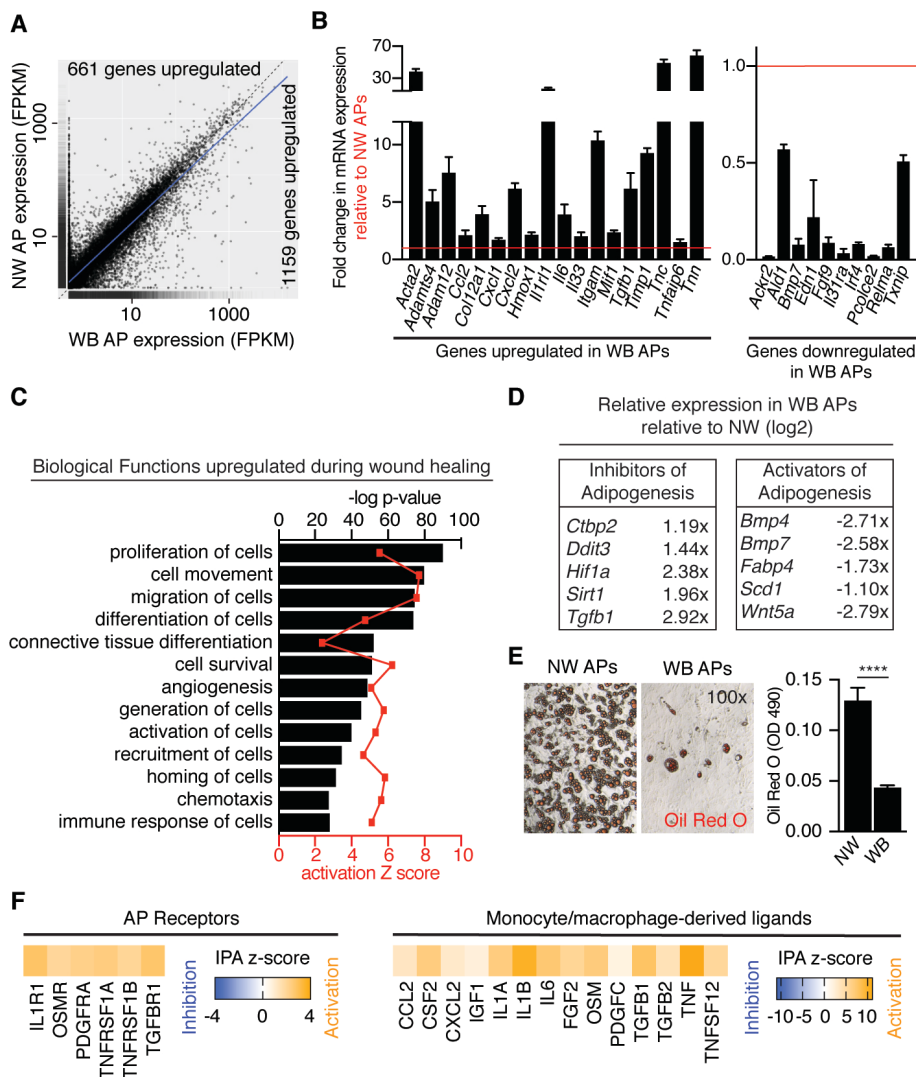


Fig. S15. AP gene expression and lineage potential are altered during wound healing. (A) FPKM scatterplot comparing gene expression profiles of non-wounded and wound bed APs. (B) Real-time qPCR quantification of gene expression in wound bed APs of genes differentially expressed in RNA-seq results. Red lines indicate expression levels in non-wounded APs. (C and D) Analysis from RNA-sequencing of non-wounded and wound bed APs. (C) Graph of biological functions altered by wound bed APs. (D) Fold change in gene expression (log2) of inhibitors and activators of adipogenesis in wound bed APs relative to non-wounded APs. (E) Oil Red O staining and quantification of *in vitro* adipogenic potential of APs from 5-day wound beds ($n = 6$) and non-wounded skin ($n = 4$) ($p < 0.0001$). (F) Ingenuity Pathway Analysis depicting activation heat maps of predicted upstream activators able to cause the observed changes in AP gene expression. All error bars indicate mean \pm SEM. NW, non-wounded; WB, 5d wound bed.

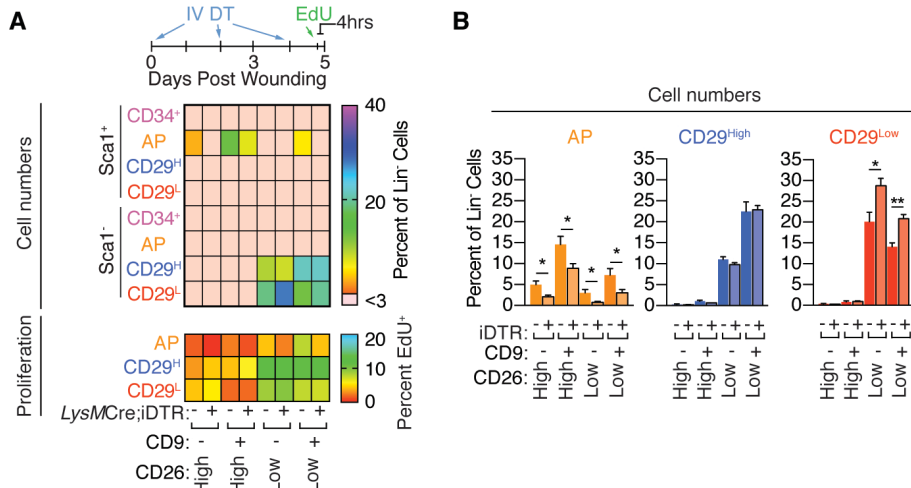


Fig. S16. Depletion of the myeloid lineage reduces AP proliferation. (A) Heat maps of relative cell numbers and the percentage of cells incorporating EdU in myeloid lineage depleted (*LysMCre;iDTR*⁺) and control (*LysMCre;iDTR*⁻) 5-day wound beds ($n = 4$). (B) Quantification of the relative abundance of AP, CD29^{High} and CD29^{Low} cell subsets in 5-day wound beds ($n = 4$). All error bars indicate mean \pm SEM. * $p < 0.05$, ** $p < 0.01$.

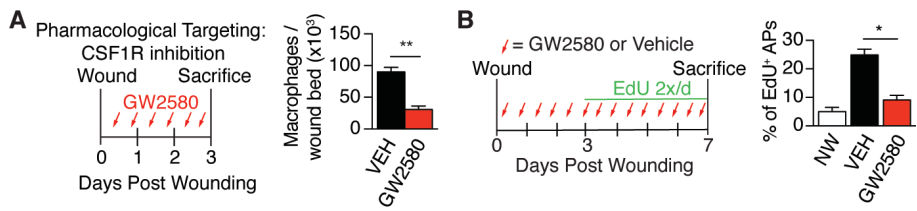


Fig. S17. CSF-1 signaling is necessary for AP proliferation. (A) Schematic and quantification of wound bed macrophages in mice treated GW2580 or vehicle control. Macrophage recruitment/maturation impairment through CSF-1R inhibition reduces wound bed macrophages in 3-day wound beds ($n = 3$, $p = 0.0031$). (B) Schematic and quantification of the percentage of APs that incorporate EdU in non-wounded (NW) skin and wound beds of mice treated GW2580 or vehicle control (VEH). GW2580 was administered twice per day using gavage feedings ($n = 3$, $p = 0.0131$). All error bars indicate mean \pm SEM.

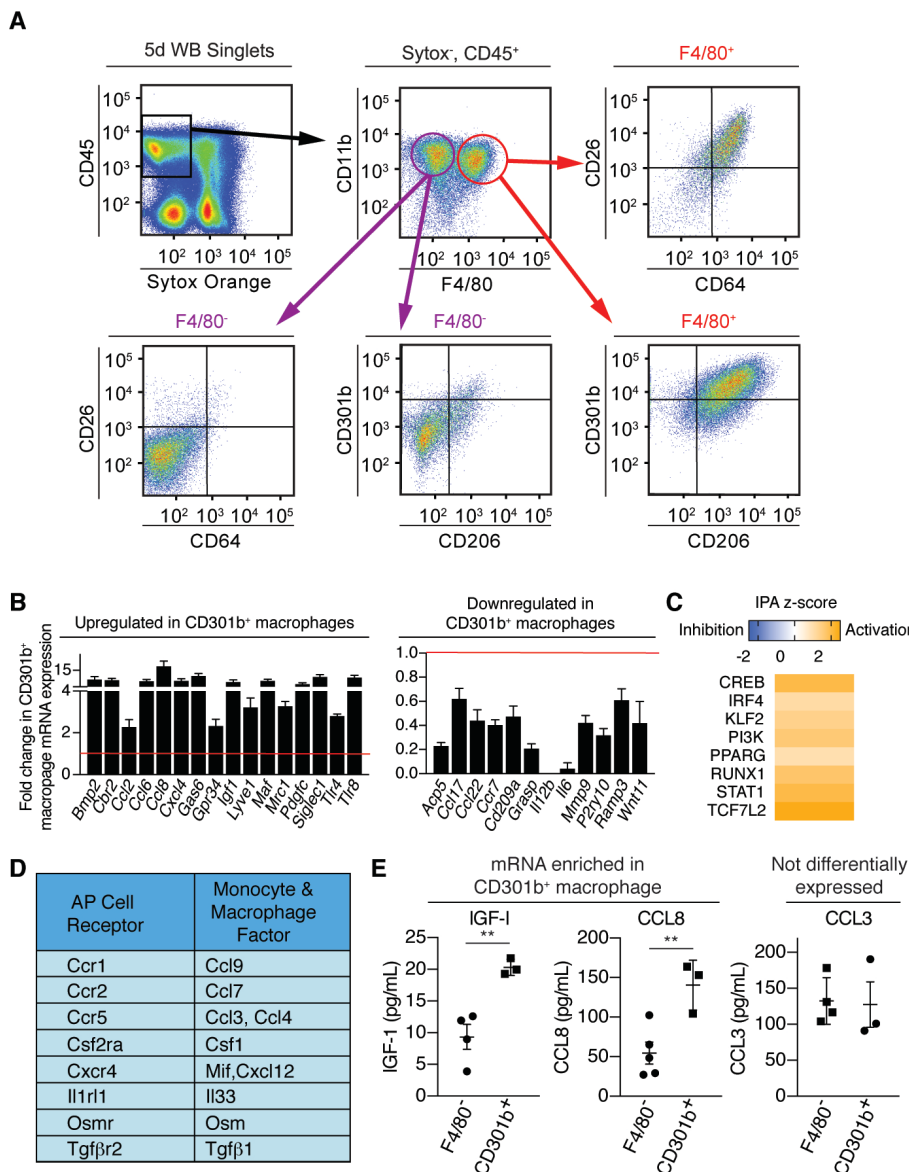


Fig. S18. Characterization of the myeloid lineage in 5-day wound beds. (A) FACS plots of surface markers that discriminate myeloid lineage cells in 5-day wound beds. The majority of CD45⁺;CD11b⁺;F4/80⁺ macrophages are CD301b⁺. (B) Real-time qPCR quantification of gene expression in 5-day wound bed CD301b⁺ macrophages compared to F4/80⁻ immune cells. Selected genes were differentially expressed in RNA-seq analysis. Red lines indicate expression levels in CD45⁺;CD11b⁺;F4/80⁻ immune cells. (C) IPA analysis revealed that changes in gene expression between CD301b⁺ macrophages and F4/80⁻ immune cells are likely due to signaling molecules involved in macrophage maturation and polarization. (D) Table of secreted molecules expressed by both CD301b⁺ macrophages and F4/80⁻ immune cells that can bind to receptors expressed by APs. (E) ELISA quantification of secreted proteins from CD301b⁺ macrophages ($n = 3$) and F4/80⁻ immune cells ($n \geq 4$). ** $p < 0.01$. All error bars indicate mean \pm SEM.

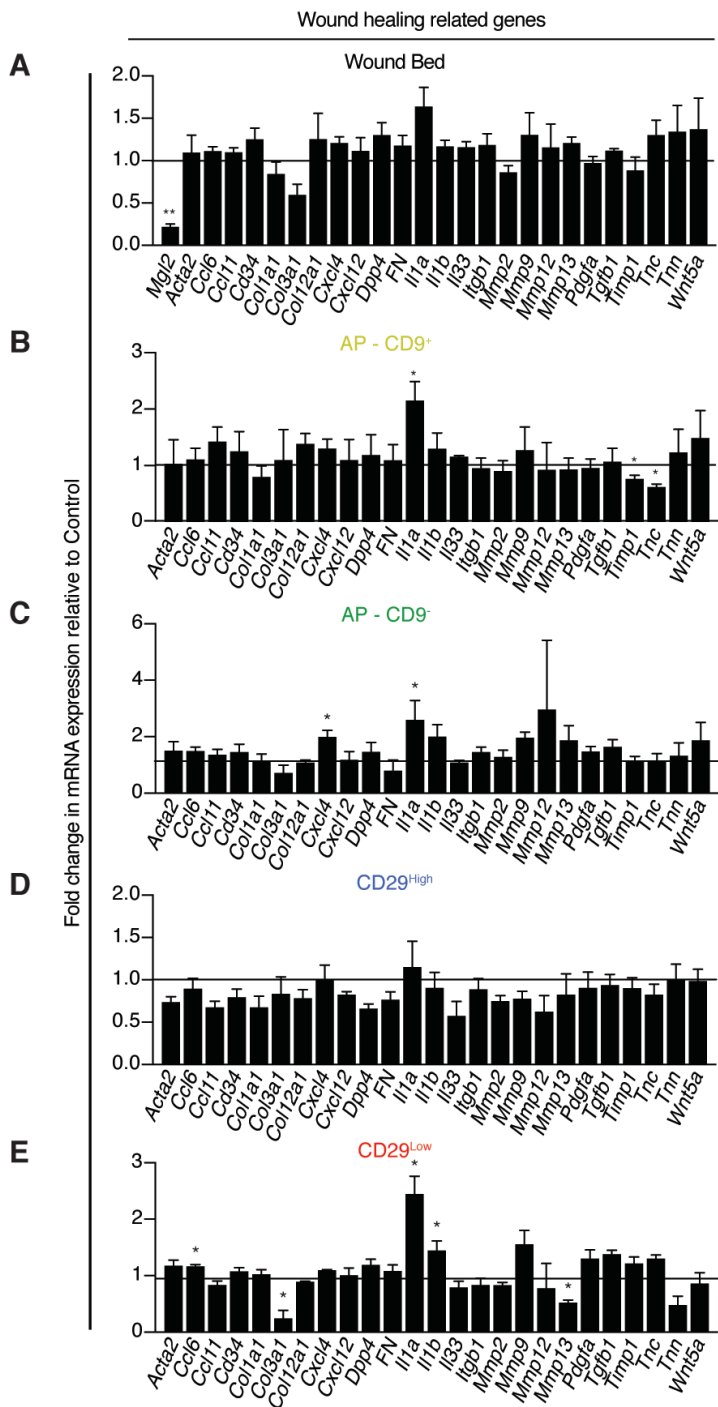


Fig. S19. CD301b⁺ macrophages do not significantly alter gene expression of myofibroblast subsets in 5-day wound beds. (A to E) Real-time PCR quantification of gene expression in 5-day wound bed mesenchymal cell subsets from Mgl2^{DTR} mice compared to control mice. Minimal changes in gene expression were detected in wound healing related genes. Black lines indicate expression levels in control mice. All error bars indicate mean \pm SEM. * $p < 0.05$, ** $p < 0.01$.

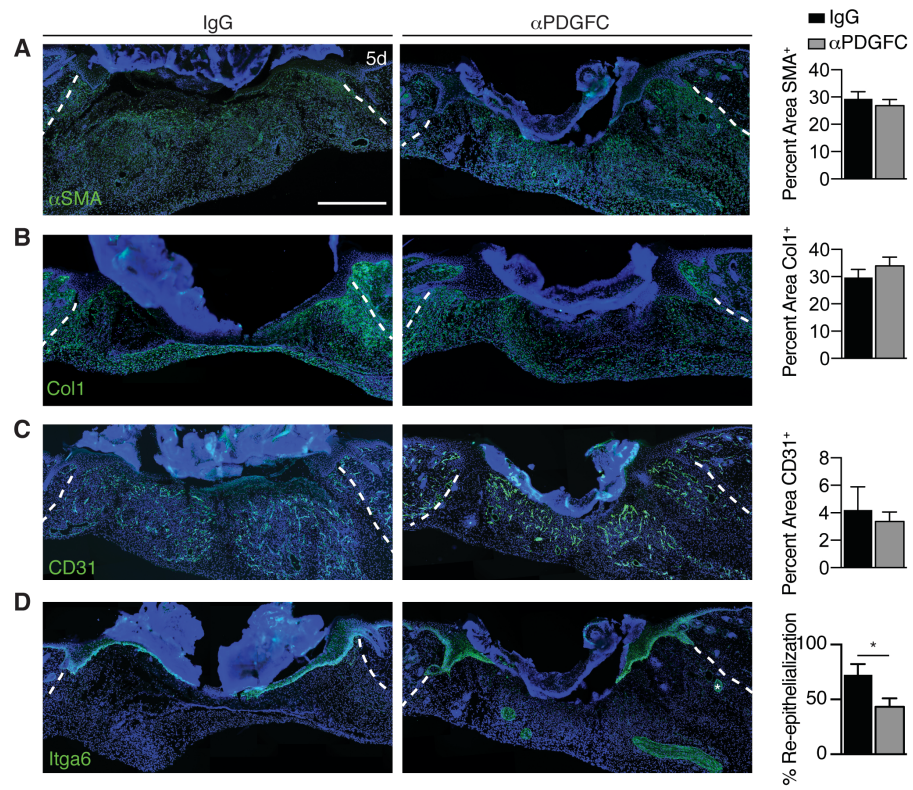


Fig. S20. Inhibition of PDGFC signaling during wound healing. (A to D) Histologic and quantitative analysis of wound bed SMA (A), Collagen I (B), revascularization (C) and re-epithelialization ($p = 0.0435$) (D) in wound beds treated with a PDGFC neutralizing antibody ($n = 8$) or IgG control ($n = 5$). White lines delineate wound edges. Scale bar, 750 μ m. All error bars indicate mean \pm SEM.

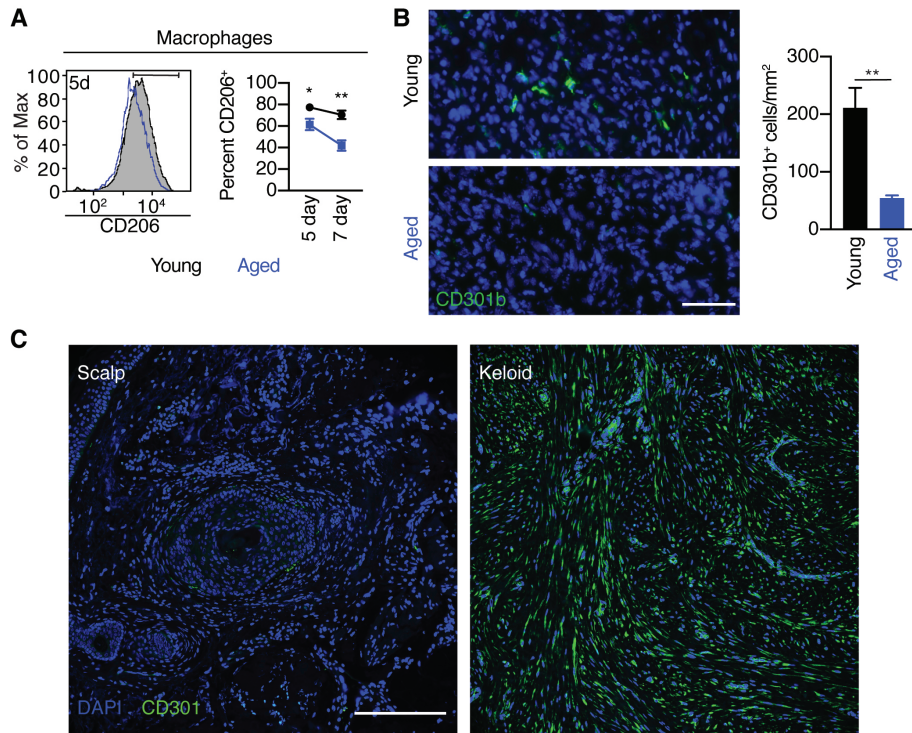


Fig. S21. CD301b⁺ macrophages are associated with fibrotic conditions. (A) Flow histogram and quantification of anti-inflammatory CD206⁺ macrophages in wound beds from young ($n = 6$) and aged ($n = 4$) mice. (B) Images and quantification of CD301b⁺ cells in day 5 wounds from young and aged mice ($n = 4$). Scale bar, 50 μ m. (C) Immunofluorescent staining of CD301 in human scalp and keloid scars. Scale bar, 200 μ m. All error bars indicate mean \pm SEM. * $p < 0.05$, ** $p < 0.01$.

Table S1. Molecule gene expression enriched in myofibroblast subsets.

Genes enriched in AP - CD9 ⁻	Relative to CD29 ^{Low}		Relative to AP - CD9 ⁺		Relative to CD29 ^{High}	
Gene Symbol (Entrez)	Expr Log Ratio	Expr p-value	Expr Log Ratio	Expr p-value	Expr Log Ratio	Expr p-value
<i>Cxcl13</i>	4.823	0.00005	2.584	0.00005	4.91	0.00005
<i>Ntrk2</i>	2.345	0.0007	2.002	0.0004	3.517	0.0002
<i>Serpina3n</i>	2.593	0.00005	1.563	0.00155	3.94	0.00005
<i>Ampd3</i>	1.941	0.00005	1.521	0.00005	2.698	0.00005
<i>Aldh1a1</i>	3.141	0.00005	1.463	0.00005	4.361	0.00005
<i>Pcdh20</i>	3.458	0.00045	1.456	0.00175	3.21	0.00135
<i>Hp</i>	1.533	0.00005	1.424	0.00005	2.474	0.00005
<i>Pt16</i>	3.804	0.00005	1.318	0.00005	5.242	0.00005
<i>Cyp1b1</i>	2.379	0.00005	1.295	0.00005	2.735	0.00005
<i>Il1r2</i>	0.865	0.0024	1.237	0.00005	2.251	0.00005
<i>Cmah</i>	2.631	0.00005	1.216	0.00005	3.351	0.00005
<i>Ak4</i>	1.327	0.0008	1.193	0.00155	1.519	0.0003
<i>Scara5</i>	4.136	0.00005	1.185	0.00005	5.349	0.00005
<i>Scn7a</i>	3.388	0.00005	1.181	0.0002	3.082	0.00005
<i>Saa3</i>	2.552	0.00005	1.169	0.00005	3.811	0.00005
<i>Dpepl</i>	2.729	0.00005	1.15	0.00005	3.482	0.00005
<i>Procr</i>	2.608	0.00005	1.147	0.00005	2.701	0.00005
<i>Aldh1a3</i>	3.203	0.00005	1.141	0.0026	3.069	0.00005
<i>Atp8b1</i>	1.816	0.00005	1.092	0.00135	1.703	0.00005
<i>Sema3c</i>	3.289	0.00005	1.087	0.00005	4.206	0.00005
<i>Ccl11</i>	3.355	0.00005	1.077	0.00005	3.788	0.00005
<i>Itih5</i>	4.247	0.00005	1.076	0.00025	4.698	0.00005
<i>Lbp</i>	3.368	0.00005	1.076	0.00005	4.685	0.00005
<i>Hegl</i>	2.727	0.00005	1.043	0.00055	2.034	0.00005
<i>Mgll</i>	2.43	0.00005	1.03	0.0005	3.406	0.00005
<i>C4b</i>	2.678	0.00005	1.003	0.00055	4.091	0.00005
<i>Prg4</i>	3.321	0.00005	0.989	0.00005	4.269	0.00005
<i>Dpy19l1</i>	1.061	0.00045	0.944	0.0017	1.607	0.00005
<i>Adm</i>	2.91	0.00005	0.916	0.00085	4.195	0.00005
<i>Il33</i>	1.954	0.00005	0.876	0.00005	2.327	0.00005
<i>Anxa3</i>	1.484	0.00005	0.844	0.0012	2.104	0.00005
<i>Il6st</i>	1.524	0.00005	0.799	0.00155	2.173	0.00005
<i>Stear4</i>	2.538	0.00005	0.751	0.00155	3.179	0.00005
<i>Gfpt2</i>	2.18	0.00005	0.684	0.00245	2.583	0.00005
<hr/>						
Genes enriched in AP - CD9 ⁺	Relative to CD29 ^{High}		Relative to AP - CD9 ⁻		Relative to CD29 ^{Low}	
Gene Symbol (Entrez)	Expr Log Ratio	Expr p-value	Expr Log Ratio	Expr p-value	Expr Log Ratio	Expr p-value
<i>Cxcl14</i>	2.699	0.00005	0.924	0.0016	1.152	0.00015
<i>Cilp</i>	1.774	0.00005	2.817	0.00005	0.837	0.0015
<i>Cyp3a13</i>	∞	0.00005	∞	0.00005	∞	0.00005
<i>Hhip12</i>	∞	0.00005	∞	0.00005	∞	0.00005
<i>Itih2</i>	∞	0.00005	∞	0.00005	∞	0.00005
<i>Wnt10b</i>	∞	0.0001	∞	0.0001	∞	0.0001
<hr/>						
Genes enriched in CD29 ^{High}	Relative to AP - CD9 ⁻		Relative to AP - CD9 ⁺		Relative to CD29 ^{Low}	
Gene Symbol (Entrez)	Expr Log Ratio	Expr p-value	Expr Log Ratio	Expr p-value	Expr Log Ratio	Expr p-value

Tnc	2.138	0.00005	1.624	0.00005	0.711	0.00275
Tpm1	2.406	0.00005	1.761	0.00005	0.774	0.00095
Lrrc15	1.499	0.00005	0.84	0.0001	0.788	0.0007
Csrp1	2.124	0.00005	1.551	0.00005	0.844	0.00025
Col12a1	1.356	0.00005	1.125	0.00005	0.908	0.00005
Vcl	1.109	0.00005	1.079	0.0001	0.947	0.00065
Rgs16	2.113	0.00005	1.446	0.00005	1.053	0.00145
Pdgfrb	1.531	0.00005	1.312	0.00005	1.073	0.0001
Wnt5a	3.452	0.00005	2.842	0.00005	1.145	0.001
Dckd	1.204	0.0001	1.086	0.00025	1.162	0.0001
Tpm2	3.421	0.00005	2.478	0.00005	1.165	0.00005
Col7a1	5.498	0.00005	4.042	0.00005	1.218	0.00005
Crabp1	5.148	0.00005	3.481	0.00005	1.261	0.00005
Ptk7	2.961	0.00005	3.442	0.0001	1.33	0.00065
Prss35	3.175	0.00005	3.281	0.00005	1.338	0.00005
Ccbe1	3.998	0.0001	3.371	0.00015	1.339	0.00135
Des	5.023	0.0015	3.702	0.00005	1.413	0.00055
Crlf1	2.839	0.00005	2.797	0.0002	1.45	0.0001
Tagln	4.735	0.00005	4.196	0.00005	1.459	0.00055
Acta2	4.065	0.00005	3.413	0.00005	1.507	0.00005
Mmp13	3.602	0.0003	2.139	0.00065	1.529	0.001
Ednra	1.67	0.00085	2.165	0.00235	1.713	0.00055
Myl9	4.787	0.00005	4.029	0.00005	1.99	0.00005
<hr/>						
Genes enriched in CD29 ^{Low}		Relative to AP - CD9 ⁻		Relative to AP - CD9 ⁺		Relative to CD29 ^{High}
Gene Symbol (Entrez)	Expr Log Ratio	Expr p-value	Expr Log Ratio	Expr p-value	Expr Log Ratio	Expr p-value
Alas2	7.844	0.00005	6.573	0.00005	5.03	0.00005
Hbb-b2	6.742	0.00005	6.359	0.00005	4.686	0.00005
Frmd4b	2.841	0.00005	2.648	0.0016	2.474	0.0002
S100a9	3.471	0.00005	2.67	0.00005	2.288	0.00005
Hdc	3.134	0.00005	2.828	0.00005	2.139	0.00005
S100a8	3.125	0.00005	2.458	0.00005	2.09	0.00005
Acta1	3.094	0.00005	3.42	0.00015	1.718	0.0001
Npl	3.913	0.00005	2.624	0.0002	1.637	0.0007
Cytip	3.717	0.0003	2.516	0.00035	1.622	0.00035
Pik3ap1	2.48	0.0023	2.244	0.0004	1.61	0.0007
Hk3	3.16	0.0004	2.807	0.00015	1.534	0.0006
Inpp5d	2.909	0.00005	2.394	0.00005	1.514	0.00005
Lcp2	2.525	0.00005	1.601	0.00005	1.505	0.0001
Hck	2.972	0.00005	2.126	0.00005	1.459	0.0004
Cyth4	3.41	0.00005	2.882	0.00005	1.447	0.00005
Ncf2	2.831	0.00005	2.236	0.00005	1.372	0.00005
Plek	3.264	0.00005	2.106	0.00005	1.35	0.00005
Pid1	1.279	0.00005	1.409	0.00005	1.348	0.00005
Lcp1	2.92	0.00005	2.197	0.00005	1.335	0.00005
Bcl2a1b	2.528	0.00005	1.98	0.00005	1.329	0.00005
Slpi	1.828	0.00005	1.723	0.00005	1.324	0.00005
Ncf1	2.589	0.00005	2.383	0.00005	1.32	0.00005
Nlrp3	3.081	0.0002	2.193	0.0002	1.301	0.00275
Fermt3	3.28	0.00005	1.823	0.00005	1.293	0.00025

Tlr13	2.619	0.00025	2.238	0.00005	1.279	0.0008
Srgn	2.219	0.00005	1.873	0.00005	1.274	0.00005
Apobec1	2.871	0.00005	1.823	0.00015	1.243	0.00075
Tpd52	3.057	0.00005	2.092	0.00005	1.241	0.00005
Rnf130	1.298	0.00005	1.29	0.00005	1.241	0.00005
Slc37a2	3.249	0.00005	1.911	0.00005	1.229	0.00015
Arg1	2.959	0.00005	2.057	0.00005	1.225	0.00005
Cybb	2.478	0.00005	1.896	0.00005	1.221	0.00015
Tgm2	0.881	0.0006	0.808	0.0014	1.193	0.00005
Coro1a	3.53	0.00005	2.487	0.00005	1.183	0.00005
Slfn2	2.18	0.00005	1.542	0.00005	1.162	0.00005
Myo1f	3.419	0.00005	1.676	0.00005	1.15	0.001
Ptpn6	3.325	0.00005	2.497	0.00005	1.149	0.0002
Lyn	2.121	0.00005	2.186	0.00005	1.135	0.00005
Lgmn	1.231	0.00005	1.229	0.00005	1.125	0.00005
Bcl2l11	1.54	0.0001	1.124	0.00135	1.111	0.00095
Renbp	1.143	0.0015	1.318	0.0003	1.109	0.00195
Ctsd	2.067	0.00005	1.569	0.00005	1.099	0.00005
Gnpda1	2.267	0.00005	1.889	0.00005	1.097	0.0019
Rac2	2.457	0.0001	2.46	0.00005	1.094	0.0019
Cbr2	3.017	0.00005	2.466	0.00005	1.09	0.00005
Pde4b	2.177	0.00005	1.688	0.00005	1.085	0.00005
Ctsb	1.109	0.00005	1.128	0.00005	1.07	0.00005
Ucp2	2.978	0.00005	2.07	0.00005	1.055	0.00005
Tmem106a	1.307	0.0001	1.117	0.00005	1.037	0.00015
Atp13a2	2.16	0.00005	1.842	0.00005	1.03	0.00135
Hmox1	1.02	0.00005	1.047	0.00005	1.023	0.00005
Atp6v0b	1.251	0.00005	1.097	0.00005	1.022	0.00005
Ctss	2.739	0.00005	1.913	0.00005	1.017	0.00005
Cflar	1.514	0.00005	1.585	0.00005	0.981	0.00115
Cyba	1.564	0.00005	1.295	0.00005	0.949	0.00025
Ctsc	2.594	0.00005	2.025	0.00005	0.936	0.0001
Unc93b1	1.741	0.00005	1.693	0.00005	0.909	0.00025
Mcl1	1.287	0.00005	1.084	0.00005	0.907	0.00015
Por	1.145	0.0001	1.467	0.00005	0.885	0.0006
Slc48a1	1.565	0.00005	1.318	0.00005	0.87	0.00145
Sqstm1	1.185	0.00005	0.851	0.0002	0.799	0.00055
Hilpda	1.518	0.00005	1.166	0.00005	0.782	0.0012
Hba-a2	6.821	0.00005	6.276	0.00005	4.535	0.00005
Mmp12	2.563	0.00005	1.832	0.00005	2.054	0.00005
Il119	1.878	0.00265	2.622	0.00125	1.755	0.002
Smpdl3a	1.291	0.00015	1.281	0.00005	1.746	0.00005
Fuca2	1.6	0.0001	1.092	0.0023	1.707	0.00005
Ccl9	3.079	0.00005	2.281	0.00005	1.564	0.00005
Lyz1	3.41	0.00005	2.393	0.00005	1.544	0.00005
Tnf	3.416	0.00005	2.434	0.00005	1.443	0.00005
Ccl4	2.874	0.00005	2.279	0.00005	1.402	0.00005
Il1a	2.735	0.00005	2.347	0.00005	1.336	0.00005
Pld4	3.064	0.00005	2.322	0.00005	1.323	0.00005
Il1b	2.657	0.00005	2.151	0.00005	1.32	0.00005

Osm	2.701	0.00005	2.429	0.00005	1.307	0.00005
Cfp	2.953	0.00005	2.269	0.00005	1.307	0.00005
Ccl6	2.697	0.00005	2.17	0.00005	1.247	0.00005
Ccl3	2.636	0.00005	2.416	0.00005	1.244	0.00005
Lgals3	1.719	0.00005	1.343	0.00005	1.213	0.00005
C1qb	3.255	0.00005	2.249	0.00005	1.185	0.00005
F13a1	2.81	0.00005	2.448	0.00005	1.177	0.00005
C1qc	3.086	0.00005	2.383	0.00005	1.142	0.00005
C1qa	3.213	0.00005	2.178	0.00005	1.137	0.00005
Il10	3.866	0.00015	2.266	0.0001	1.129	0.0023
Cxcl2	1.338	0.00005	0.998	0.00005	1.106	0.00005
Il1rn	2.427	0.00005	2.396	0.00005	1.092	0.00005
Apoe	3.099	0.00005	2.182	0.00005	1.047	0.00005
Bpgm	2.079	0.00005	1.989	0.00005	1.036	0.00045
Pla2g7	2.898	0.00005	2.181	0.00005	1.027	0.0001
Pf4	2.895	0.00005	2.04	0.00005	1.018	0.00005
Trf	1.021	0.0002	1.131	0.00005	1.01	0.0001
Cxcl3	1.623	0.00005	1.186	0.00005	0.857	0.00025
Grn	0.897	0.00005	0.838	0.00025	0.77	0.00065
Akna	2.231	0.00095	2.172	0.00195	2.094	0.0026
Irf5	2.521	0.00005	2.782	0.00005	1.47	0.00005
Fgr	2.042	0.0001	2.074	0.0002	1.452	0.0016
Fli1	2.033	0.00155	1.725	0.0005	1.346	0.002
Samsn1	3.097	0.00005	2.565	0.0002	1.302	0.00065
Mxd1	1.943	0.00005	1.693	0.00005	1.165	0.00005
Mafb	2.463	0.00005	1.608	0.00005	1.09	0.00005
Neat1	1.339	0.00005	1.645	0.00005	1.043	0.0001
Creg1	0.982	0.0002	0.842	0.00095	0.973	0.0002
Tgif1l	1.12	0.00005	0.922	0.0004	0.945	0.0005
Nfkbie	1.617	0.00005	1.208	0.00015	0.938	0.00205
Nfkbid	2.68	0.00005	2.221	0.00005	0.934	0.0013
Mdm2	1.071	0.00005	0.922	0.00145	0.91	0.00065
Btg1	0.805	0.0004	0.84	0.0002	0.701	0.00255
Slfn4	3.244	0.00005	2.142	0.00005	1.349	0.00005
Ms4a6d	2.941	0.00005	2.048	0.00005	1.347	0.00005
Mkrn1	1.485	0.00005	1.061	0.00055	1.245	0.0001
Ms4a7	2.978	0.00005	2.232	0.00005	1.244	0.00005
Ms4a6b	3.615	0.00005	2.46	0.00005	1.228	0.0002
Rassf4	2.632	0.00005	2.684	0.00005	1.204	0.0016
Gm6377	3.88	0.00035	2.03	0.0001	1.182	0.00175
Clec4a3	2.226	0.0001	1.823	0.00005	1.135	0.00065
Fam105a	2.872	0.00005	1.863	0.00005	1.119	0.00065
Efh2d	1.844	0.00005	1.674	0.00005	1.101	0.00005
Grina	1.156	0.00005	1.357	0.00005	0.987	0.0005
Rasgef1b	2.075	0.00005	1.876	0.00005	0.974	0.0002
Lhfpl2	1.004	0.00065	1.076	0.00015	0.858	0.00175
Aplnr	3.718	0.0003	3.721	0.00045	2.823	0.0001
Cd163	3.315	0.00155	3.652	0.0027	2.111	0.00015
Cd300lf	3.553	0.0002	2.726	0.002	2.054	0.00035
Cd300lb	1.734	0.00075	2.542	0.00135	2.042	0.0001

Susd3	2.484	0.0002	2.407	0.0003	1.983	0.00095
Olr1	2.036	0.00015	2.057	0.00005	1.814	0.00005
Bst1	2.732	0.00005	2.311	0.00045	1.787	0.0003
Nfam1	2.215	0.0001	1.954	0.0002	1.721	0.0002
Ccr1	2.993	0.00005	2.078	0.00005	1.668	0.00005
Cd38	2.342	0.00005	2.329	0.00005	1.64	0.00005
Csf3r	2.94	0.00005	2.753	0.0001	1.631	0.00005
Clec4e	3.101	0.00005	2.302	0.00005	1.606	0.00005
Trem1	2.337	0.00005	2.143	0.00005	1.56	0.00015
Fcrls	2.591	0.00005	2.329	0.00005	1.551	0.00005
Tyrobp	3.258	0.00005	2.337	0.00005	1.509	0.00005
Tmem37	2.984	0.00005	2.595	0.00005	1.494	0.0003
Lair1	3.273	0.0008	2.166	0.00015	1.469	0.00035
Cd36	2.968	0.00005	2.093	0.00005	1.464	0.00005
Clec4n	2.947	0.00005	2.537	0.00005	1.458	0.00005
Dpep2	2.886	0.00005	2.193	0.00005	1.426	0.0002
Cd86	3.817	0.00015	2.574	0.00005	1.424	0.0011
Mrc1	2.324	0.00005	2.299	0.00005	1.41	0.00005
Pecam1	3.103	0.00145	3.328	0.0007	1.405	0.00285
Slc7a8	1.131	0.0017	1.188	0.00115	1.399	0.0002
Msr1	3.44	0.00005	2.416	0.00005	1.393	0.0005
Cd83	3.359	0.00005	2.292	0.00005	1.387	0.00005
Dab2	1.59	0.00005	1.334	0.00005	1.372	0.00005
Stxbp2	2.552	0.0002	1.837	0.00135	1.37	0.00265
Dok2	3.113	0.00025	2.285	0.00005	1.364	0.0002
Cd300ld	2.993	0.00005	2.272	0.00005	1.364	0.0001
Csf2rb	3.928	0.00005	2.855	0.00005	1.362	0.00015
Plvap	3.277	0.00005	2.88	0.00005	1.347	0.00005
Fcgr1	2.298	0.00005	1.998	0.00005	1.331	0.00005
Cd14	2.785	0.00005	2.108	0.00005	1.327	0.00005
Clec4a2	3.066	0.00005	2.83	0.00005	1.326	0.00025
Ptprc	2.521	0.00005	1.903	0.00005	1.291	0.00005
Slc43a2	3.433	0.00005	1.999	0.00005	1.288	0.0005
Ccrl2	2.611	0.00005	2.025	0.00005	1.28	0.00005
C5ar1	2.98	0.00005	2.209	0.00005	1.275	0.00005
Trem2	3.634	0.00005	2.278	0.00005	1.273	0.00005
Itgam	2.967	0.00005	2.231	0.00005	1.268	0.00005
Folr2	2.875	0.00005	2.471	0.00005	1.265	0.00005
Cd93	2.388	0.00005	2.636	0.00005	1.251	0.00015
Clec4d	2.92	0.00005	2.035	0.00005	1.233	0.00005
Alox5ap	3.086	0.00005	2.331	0.00005	1.222	0.00005
Lat2	2.964	0.00005	2.748	0.00005	1.168	0.0007
Cd68	3.178	0.00005	2.328	0.00005	1.164	0.00005
Tnfrsf1b	1.708	0.00005	1.409	0.00005	1.155	0.00005
Selplg	3.6	0.00005	2.239	0.00005	1.136	0.0002
Fcgr3	2.907	0.00005	2.064	0.00005	1.11	0.00005
Tlr2	1.736	0.00005	1.835	0.00005	1.106	0.00005
Slc11a1	2.843	0.00005	2.403	0.00005	1.089	0.0001
Itgb2	2.756	0.00005	2.175	0.00005	1.088	0.00005
Adam8	2.538	0.00005	2.116	0.00005	1.055	0.00005

Cd300a	2.942	0.00005	2.101	0.00005	1.054	0.00265
Ccr5	2.549	0.00005	2.026	0.00005	1.04	0.00065
Tmem8	2.713	0.00005	2.594	0.00005	1.029	0.0021
Nckap11	2.445	0.00005	1.998	0.00005	1.016	0.0014
Ninj1	2.086	0.00005	1.403	0.00005	1.003	0.00015
Entpd1	2.816	0.00005	2.222	0.00005	0.994	0.00115
Clec7a	2.757	0.00005	1.549	0.00005	0.988	0.0019
Fegr2b	2.536	0.00005	1.971	0.00005	0.985	0.00015
Csf1r	1.445	0.00005	1.213	0.00005	0.982	0.0001
Flrt3	1.468	0.00015	1.265	0.0001	0.965	0.00135
Cd53	2.428	0.00005	1.983	0.00005	0.948	0.0002
Feer1g	2.855	0.00005	2.071	0.00005	0.944	0.0001
Ezr	2.227	0.00005	1.191	0.0003	0.938	0.00255
Kctd12	2.246	0.00005	1.629	0.00005	0.907	0.00265
Ccr2	2.314	0.00005	2.166	0.00005	0.889	0.0028
Laptm5	2.411	0.00005	1.966	0.00005	0.862	0.00035
Ehd4	1.666	0.00005	1.523	0.00005	0.816	0.00295

Genes enriched in APs	AP - CD9 ⁺				AP - CD9 ⁻			
	Relative to CD29 ^{Low}		Relative to CD29 ^{High}		Relative to CD29 ^{Low}		Relative to CD29 ^{High}	
Gene Symbol (Entrez)	Expr Log Ratio	Expr p-value	Expr Log Ratio	Expr p-value	Expr Log Ratio	Expr p-value	Expr Log Ratio	Expr p-value
Abi3bp	1.155	0.00005	1.384	0.00005	1.291	0.00005	1.52	0.00005
Ace	2.015	0.00005	3.576	0.00005	2.547	0.00005	4.109	0.00005
Adamts1	1.263	0.00005	2.095	0.00005	1.514	0.00005	2.346	0.00005
Adamts15	2.049	0.00005	3.774	0.00005	2.4	0.00005	4.125	0.00005
Adamts4	1.233	0.00005	1.074	0.00005	1.491	0.00005	1.332	0.00005
Adamts5	2.023	0.00005	2.471	0.00005	2.707	0.00005	3.155	0.00005
Adamtsl1	1.335	0.00005	1.625	0.00005	1.702	0.00005	1.991	0.00005
Add3	1.027	0.0006	1.676	0.00005	1.436	0.00005	2.085	0.00005
Akr1c18	3.019	0.00005	4.304	0.0003	3.506	0.00005	4.791	0.00005
Apod	1.948	0.00005	3.234	0.00005	2.231	0.00005	3.516	0.00005
Arhgap29	1.199	0.0012	1.664	0.00005	1.669	0.00005	2.134	0.00005
Arsi	1.296	0.00005	2.193	0.00005	1.708	0.00005	2.605	0.00005
Axl	1.344	0.00005	1.074	0.00005	1.688	0.00005	1.417	0.00005
Bicc1	0.946	0.0007	1.108	0.0001	1.303	0.00005	1.465	0.00005
Bmper	1.314	0.00045	2.117	0.00005	1.767	0.00005	2.57	0.00005
C2	1.227	0.00005	2.214	0.00005	1.776	0.00005	2.763	0.00005
C3	2.07	0.00005	3.476	0.00005	3.156	0.00005	4.562	0.00005
Ccdc80	1.124	0.00005	1.677	0.00005	1.534	0.00005	2.086	0.00005
Ccl2	1.194	0.00005	1.789	0.00005	1.289	0.00005	1.883	0.00005
Ccl7	1.267	0.00005	1.779	0.00005	1.715	0.00005	2.227	0.00005
Cd164	0.814	0.00065	0.792	0.0008	1.15	0.00005	1.128	0.00005
Cd248	1.69	0.00005	1.356	0.00005	1.863	0.00005	1.528	0.00005
Cd34	1.92	0.00005	3.025	0.00005	2.525	0.00005	3.629	0.00005
Cd55	2.277	0.00005	2.169	0.00005	2.542	0.00005	2.435	0.00005
Cebpd	1.848	0.00005	1.812	0.00005	2.267	0.00005	2.23	0.00005
Cercam	1.073	0.0001	0.984	0.0002	1.263	0.00005	1.175	0.00005
Ces2g	1.639	0.0001	2.946	0.00005	1.869	0.00005	3.175	0.00005
Cfb	1.453	0.00005	2.578	0.00005	2.08	0.00005	3.205	0.00005
Chl1	1.739	0.00005	3.586	0.00005	2.417	0.00005	4.264	0.00005

Chrd1	1.478	0.00005	3.018	0.00005	2.15	0.00005	3.691	0.00005
Cldn10	2.172	0.00015	2.219	0.0001	2.783	0.00005	2.83	0.00005
Clec3b	3.418	0.00005	4.113	0.00005	4.134	0.00005	4.829	0.00005
Col14a1	1.581	0.00005	2.838	0.00005	2.021	0.00005	3.278	0.00005
Col4a5	2.338	0.00005	2.179	0.00075	2.395	0.00005	2.235	0.00065
Col5a2	0.781	0.0009	0.731	0.00195	0.764	0.0013	0.714	0.0027
Cp	2.004	0.00015	1.934	0.00005	2.192	0.00005	2.122	0.00005
Cpxm1	0.846	0.0002	1.217	0.00005	1.22	0.00005	1.592	0.00005
Cpz	1.413	0.00005	1.717	0.00005	1.803	0.00005	2.106	0.00005
Cthrc1	1.146	0.00005	1.122	0.00005	1.275	0.00005	1.251	0.00005
Ctsf	1.374	0.0013	1.652	0.00035	1.715	0.00005	1.994	0.0001
Cxcl10	1.604	0.00005	1.674	0.00005	2.283	0.00005	2.353	0.00005
Cxcl12	0.758	0.00135	1.047	0.0001	1.141	0.00005	1.43	0.00005
Cygb	1.712	0.00005	1.786	0.00005	1.837	0.00005	1.911	0.00005
Cyr61	1.439	0.00005	1.66	0.00005	1.483	0.00005	1.704	0.00005
Dapk1	1.217	0.0015	3.046	0.00005	1.467	0.00015	3.295	0.00005
Dcn	1.387	0.00005	1.736	0.00005	1.794	0.00005	2.143	0.00005
Ddr2	0.999	0.00015	0.892	0.0003	1.536	0.00005	1.429	0.00005
Dmkn	2.036	0.00005	3.025	0.00005	1.965	0.00005	2.954	0.00005
Dpp4	1.984	0.00005	3.284	0.00005	2.31	0.00005	3.61	0.00005
Dpt	1.346	0.00005	2.121	0.00005	1.623	0.00005	2.398	0.00005
Dsel	1.125	0.0004	1.291	0.00025	0.973	0.0023	1.14	0.0006
Efemp1	1.878	0.00005	3.148	0.00005	2.067	0.00005	3.337	0.00005
Efemp2	0.942	0.00015	0.88	0.00015	1.071	0.00005	1.01	0.00005
Egfr	1.936	0.00005	1.541	0.00005	2.382	0.00005	1.987	0.00005
Egr1	0.79	0.0009	0.752	0.00145	0.875	0.00015	0.837	0.00035
Entpd2	1.555	0.00115	2.237	0.00035	2.198	0.00005	2.88	0.00005
Epdr1	1.384	0.00005	1.696	0.00005	1.229	0.00005	1.541	0.00005
Errf1	0.988	0.00005	1.574	0.00005	1.391	0.00005	1.977	0.00005
Fam102a	2.16	0.00005	2.021	0.00005	2.129	0.00005	1.99	0.00005
Fam162a	0.9	0.00035	0.897	0.00055	0.932	0.0001	0.929	0.00015
Fbln1	1.159	0.00005	1.141	0.00005	1.673	0.00005	1.656	0.00005
Fbn1	1.298	0.00005	1.25	0.00005	1.523	0.00005	1.475	0.00005
Fgl1	∞	0.00005	∞	0.00005	∞	0.00005	∞	0.00005
Fgl2	1.177	0.00005	2.339	0.00005	1.887	0.00005	3.05	0.00005
Fhl1	1.106	0.00055	1.701	0.00005	1.052	0.001	1.647	0.00005
Fkbp7	0.777	0.00205	0.766	0.0022	0.874	0.00065	0.863	0.0005
Fkbp9	0.776	0.00075	0.725	0.0018	0.91	0.00015	0.859	0.0002
Flrt2	1.444	0.00005	1.634	0.00005	2.13	0.00005	2.32	0.00005
Fndc1	1.106	0.00005	1.223	0.00005	1.481	0.00005	1.598	0.00005
Fst	0.978	0.00015	1.345	0.00005	1.294	0.00005	1.661	0.00005
Fstl1	1.248	0.00005	1.193	0.00005	1.45	0.00005	1.395	0.00005
Fxyd1	1.845	0.0002	2.533	0.00005	2.062	0.00005	2.75	0.00005
Gabra3	1.494	0.0026	2.735	0.00105	2.116	0.00005	3.356	0.00015
Gbp3	1.47	0.0001	1.926	0.00005	1.526	0.0001	1.982	0.00005
Gem	1.113	0.00005	1.468	0.00005	1.22	0.00005	1.575	0.00005
Ggcx	1.038	0.00035	0.827	0.003	1.065	0.00025	0.854	0.0022
Gja1	0.809	0.0005	1.199	0.00005	1.045	0.00005	1.435	0.00005
Gpc3	2.051	0.00005	2.552	0.00005	2.301	0.00005	2.802	0.00005
Gpr153	1.125	0.00005	0.987	0.00015	1.134	0.00005	0.996	0.00015

Gpx3	0.811	0.00095	0.938	0.00025	1.059	0.00015	1.186	0.00005
Gsn	1.425	0.00005	1.788	0.00005	2.028	0.00005	2.391	0.00005
Gstm2	1.014	0.00005	0.889	0.00065	1.488	0.00005	1.363	0.00005
Has1	2.335	0.00005	3.116	0.00005	2.65	0.00005	3.432	0.00005
Hes1	1.044	0.00195	1.202	0.00045	1.338	0.00005	1.497	0.00005
Higd1a	1.081	0.0001	0.857	0.00115	1.145	0.0001	0.921	0.0005
Hpgd	1.95	0.0015	2.033	0.00305	2.452	0.00005	2.535	0.00055
Hspg2	1.262	0.00005	0.811	0.00235	1.408	0.00005	0.957	0.00025
Htra3	2.193	0.00005	2.34	0.00005	2.506	0.00005	2.652	0.00005
Id3	0.963	0.00025	1.154	0.00005	1.466	0.00005	1.657	0.00005
Ifi205	1.471	0.00005	2.282	0.00005	1.842	0.00005	2.653	0.00005
Igfbp4	0.814	0.0009	1.701	0.00005	1.254	0.00005	2.141	0.00005
Igfbp5	1.177	0.00005	1.691	0.00005	0.961	0.0004	1.475	0.00005
Igfbp6	1.227	0.00005	2.035	0.00005	1.097	0.00005	1.904	0.00005
Iigp1	2.035	0.00005	2.3	0.00005	2.336	0.00005	2.602	0.00005
Il11ra1	1.339	0.00005	1.818	0.00005	1.718	0.00005	2.197	0.00005
Il6	2.447	0.00005	2.662	0.00005	2.982	0.00005	3.198	0.00005
Irak3	1.312	0.00005	1.853	0.00005	1.85	0.00005	2.39	0.00005
Irf7	0.864	0.0009	1.255	0.00005	1.066	0.00005	1.457	0.00005
Islr	1.994	0.00005	2.101	0.00005	2.54	0.00005	2.647	0.00005
Itpkc	1.241	0.00005	1.436	0.00005	1.311	0.00005	1.507	0.00005
Jak1	0.739	0.00245	1.034	0.00005	0.919	0.00015	1.213	0.00005
Jund	0.752	0.00115	0.758	0.00115	0.682	0.0024	0.688	0.0021
Kdelc2	0.965	0.00165	0.876	0.0022	1.406	0.00005	1.317	0.00005
Klf4	1.341	0.00005	1.296	0.00005	1.532	0.00005	1.487	0.00005
Lama2	1.188	0.00215	1.403	0.001	1.734	0.00005	1.949	0.00005
Lama4	0.794	0.00115	0.775	0.0027	1.26	0.00005	1.241	0.00005
Lamb2	1.089	0.00005	1.528	0.00005	1.335	0.00005	1.773	0.00005
Lamc1	0.868	0.00035	0.975	0.00005	1.235	0.00005	1.342	0.00005
Lgi2	1.025	0.0022	1.426	0.0003	1.229	0.0003	1.63	0.0001
Lhfp	0.955	0.00025	0.765	0.0017	1.24	0.00005	1.051	0.0001
Lima1	0.939	0.0004	0.925	0.0001	1.076	0.00005	1.063	0.00005
Lox	1.032	0.00005	1.445	0.00005	1.332	0.00005	1.745	0.00005
Lrrc17	0.836	0.0003	0.933	0.00005	0.853	0.0003	0.95	0.0001
Lrrn4cl	2.502	0.00005	3.238	0.00005	2.916	0.00005	3.652	0.00005
Lum	1.236	0.00005	1.729	0.00005	1.236	0.00005	1.729	0.00005
Ly6c1	2.264	0.00005	3.338	0.00005	2.815	0.00005	3.889	0.00005
Mfap5	1.228	0.00005	1.366	0.00005	1.409	0.00005	1.547	0.00005
Mgst1	1.044	0.00005	1.147	0.00005	1.346	0.00005	1.448	0.00005
Mmp2	0.989	0.00005	1.322	0.00005	1.302	0.00005	1.635	0.00005
Mmp23	0.758	0.00215	0.918	0.00045	0.933	0.00025	1.093	0.00005
Mmp27	1.798	0.00075	2.245	0.00035	2.501	0.00005	2.948	0.00005
Mmp3	1.499	0.00005	2.776	0.00005	2.145	0.00005	3.422	0.00005
Mt1	1.234	0.00005	1.607	0.00005	1.335	0.00005	1.709	0.00005
Mt2	1.513	0.00005	1.911	0.00005	1.766	0.00005	2.164	0.00005
Myc	1.675	0.00005	1.731	0.00005	1.976	0.00005	2.032	0.00005
Ndn	1.049	0.00025	1.001	0.0005	1.284	0.00005	1.235	0.00005
Ndrg4	1.111	0.00005	1.388	0.00005	0.945	0.0004	1.222	0.00005
Ndufa4l2	1.5	0.00005	1.288	0.0004	1.506	0.00005	1.294	0.0004
Nid1	1.003	0.00005	1.261	0.00005	1.435	0.00005	1.693	0.00005

Nod1	1.195	0.002	1.19	0.00215	1.445	0.0004	1.439	0.00035
Nos2	1.234	0.00015	1.276	0.00005	1.788	0.00005	1.83	0.00005
Nov	2.223	0.00005	3.059	0.00005	1.523	0.00005	2.359	0.00005
Nucb2	0.831	0.0018	0.968	0.00015	1.284	0.00005	1.42	0.00005
Nuprl	0.955	0.00045	0.994	0.00015	0.935	0.00045	0.974	0.00015
Ogn	1.916	0.00055	2.554	0.00025	2.569	0.00005	3.207	0.00005
Olfml2b	1.204	0.00005	1.399	0.00005	1.514	0.00005	1.709	0.00005
Osr1	1.644	0.00005	1.81	0.00005	2.153	0.00005	2.319	0.00005
Osr2	1.696	0.00005	1.772	0.00005	1.786	0.00005	1.862	0.00005
P4ha1	0.797	0.00065	0.761	0.00095	0.916	0.00005	0.88	0.00005
Pamr1	1.894	0.00045	2.771	0.0008	2.439	0.00005	3.315	0.00005
Pcolce	0.847	0.0003	0.793	0.00055	1.078	0.00005	1.024	0.00005
Pcolce2	1.696	0.0001	1.576	0.0002	2.325	0.00005	2.205	0.00005
Pcsk5	1.038	0.00005	1.502	0.00005	1.362	0.00005	1.825	0.00005
Pcsk6	2.101	0.00005	4.463	0.0023	1.935	0.0004	4.297	0.00275
Pdgfra	0.967	0.00005	1.409	0.00005	1.1	0.00005	1.542	0.00005
Phlda1	0.958	0.0002	0.982	0.0002	0.888	0.0008	0.956	0.0002
Plac8	1.018	0.0004	1.038	0.00035	1.725	0.00005	1.745	0.00005
Plagl1	1.627	0.00005	1.723	0.00005	2.104	0.00005	2.2	0.00005
Plat	1.034	0.00005	1.018	0.00005	1.427	0.00005	1.411	0.00005
Plod2	1.003	0.00005	1.351	0.00005	0.961	0.00005	1.309	0.00005
Pnp	0.924	0.00045	1.139	0.00015	1.261	0.00005	1.535	0.0006
Podn	1.899	0.00005	2.581	0.00005	1.885	0.00005	2.567	0.00005
Prelp	1.712	0.00005	2.498	0.00005	1.963	0.00005	2.749	0.00005
Prnp	0.818	0.0013	1.25	0.00005	1.027	0.00005	1.459	0.00005
Prss23	1.644	0.00005	2.136	0.00005	2.063	0.00005	2.555	0.00005
Ptgis	1.315	0.00005	2.02	0.00005	1.675	0.00005	2.38	0.00005
Ptx3	2.605	0.00005	3.431	0.00005	3.249	0.00005	4.075	0.00005
Rarres2	0.758	0.0016	0.882	0.00005	1.133	0.00005	1.256	0.00005
Rcan1	1.081	0.00005	1.927	0.00005	0.873	0.0001	1.719	0.00005
Rdh10	1.391	0.00005	1.515	0.00005	1.453	0.00005	1.577	0.00005
Rhoj	1.198	0.00005	1.145	0.00005	1.575	0.00005	1.522	0.00005
Rnd1	2.179	0.00005	2.783	0.00005	2.646	0.00005	3.249	0.00005
S100a16	0.994	0.00005	1.241	0.00005	1.229	0.00005	1.476	0.00005
Sbsn	1.597	0.0004	2.255	0.00005	1.725	0.00025	2.383	0.00005
Scara3	1.192	0.00005	1.912	0.00005	1.654	0.00005	2.374	0.00005
Sema3b	1.778	0.00005	2.704	0.00005	1.912	0.00005	2.838	0.00005
Serpib1a	0.821	0.0016	1.736	0.00005	0.942	0.00045	1.857	0.00005
Serpib2	0.792	0.00045	1.244	0.00005	1.347	0.00005	1.798	0.00005
Serpib7	∞	0.00005	∞	0.00005	∞	0.00005	∞	0.00005
Serpine1	1.704	0.00005	1.154	0.00005	2.071	0.00005	1.522	0.00005
Serpine1	1.486	0.00005	2.085	0.00005	2.138	0.00005	2.736	0.00005
Sfrp2	1.502	0.00005	2.132	0.00005	1.354	0.00005	1.984	0.00005
Sfrp4	2.034	0.00005	4.023	0.00005	1.657	0.00005	3.646	0.00005
Sgce	1.72	0.00005	1.341	0.00005	1.872	0.00005	1.492	0.00005
Sgpp1	0.886	0.0015	0.903	0.00135	1.267	0.00005	1.285	0.00005
Slc10a6	1.909	0.00005	2.767	0.00005	2.622	0.00005	3.48	0.00005
Slc22a18	∞	0.00005	∞	0.00005	∞	0.0001	∞	0.0001
Slc39a14	1.097	0.00005	1.287	0.00005	1.607	0.00005	1.796	0.00005
Slc43a3	1.758	0.00005	1.625	0.00005	2.286	0.00005	2.153	0.00005

Slfn5	1.044	0.00075	1.48	0.00005	1.607	0.00005	2.043	0.00005
Sned1	1.474	0.0008	2.889	0.0007	2.034	0.00005	3.449	0.00005
Socs1	1.449	0.00005	1.494	0.00005	1.682	0.00005	1.727	0.00005
Socs3	0.97	0.00005	1.192	0.00005	1.247	0.00005	1.468	0.00005
Sod3	1.049	0.00005	0.899	0.00005	1.295	0.00005	1.145	0.00005
Spsb1	1.066	0.0001	1.037	0.0001	1.69	0.00005	1.661	0.00005
Spx	1.004	0.0003	1.341	0.00005	1.478	0.00005	1.815	0.00005
Steap3	1.059	0.00235	1.519	0.0003	1.986	0.00005	1.257	0.00005
Sulf1	1.227	0.00005	0.87	0.00025	1.539	0.00005	1.182	0.00005
Svep1	1.618	0.00005	2.13	0.00005	2.312	0.00005	2.823	0.00005
Tgfb2	1.046	0.00005	1.516	0.00005	1.25	0.00005	1.72	0.00005
Tgfb3	0.869	0.0008	1.558	0.00005	1.096	0.00005	1.785	0.00005
Thbs3	1.099	0.00005	1.39	0.00005	1.044	0.00015	1.335	0.00005
Timp1	0.992	0.0001	0.969	0.00015	1.288	0.00005	1.266	0.00005
Timp3	0.97	0.0003	1.005	0.0003	1.304	0.00005	1.339	0.00005
Tiparp	0.861	0.0012	1.343	0.00005	1.184	0.00005	1.666	0.00005
Tmeff2	2.294	0.00005	3.576	0.00005	2.707	0.00005	3.989	0.00005
Tmem100	2.003	0.0001	2.32	0.00005	2.448	0.00005	2.765	0.00005
Tmem45a	1.316	0.00005	1.192	0.00005	1.484	0.00005	1.359	0.00005
Tnfaip6	2.064	0.00005	2.214	0.00005	2.312	0.00005	2.463	0.00005
Tnxb	3.142	0.00005	3.534	0.00005	3.343	0.00005	3.735	0.00005
Twsg1	1.034	0.0003	1.001	0.0002	1.362	0.00005	1.329	0.00005
Uap1	1.588	0.00005	1.907	0.00005	2.062	0.00005	2.381	0.00005
Ugdh	1.466	0.00005	1.881	0.00005	1.966	0.00005	2.381	0.00005
Ugp2	0.852	0.00095	1.533	0.00005	1.003	0.00005	1.683	0.00005
Vcam1	0.919	0.00035	1.348	0.00005	0.807	0.00115	1.236	0.00005
Vit	∞	0.00005	∞	0.00005	∞	0.00005	∞	0.00005
Wdr92	1.027	0.0001	1.053	0.00005	1.637	0.00005	1.663	0.00005
Wisp2	1.374	0.00005	2.178	0.00005	1.715	0.00005	2.519	0.00005
Wnt2	1.408	0.00005	2.057	0.00005	1.579	0.00005	2.228	0.00005
Zfp36	0.784	0.00155	0.89	0.0002	0.982	0.00015	1.088	0.00005
Zfp36l1	0.886	0.0008	1.145	0.00005	1.211	0.00005	1.469	0.00005

Table S2. Ingenuity Pathway Analysis of predicted upstream activators for each gene expression profile (z-score ≥ 2).

Predicted Upstream Regulators of CD29 ^{High} Gene Expression Profile			
Upstream regulators	Relative to CD29 ^{Low}	Relative to AP - CD9 ⁺	Relative to AP - CD9 ⁻
TGFB1	3.668120633	5.716474286	5.953360301
D-glucose	3.197083529	3.963318679	5.109107592
SMARCA4	2.400396793	4.474063035	4.79075795
hydrogen peroxide	2.189378817	3.665678374	4.270226722
SP1	2.40766193	3.557920549	3.829316006
AGT	2.411764706	3.4278376	3.892109562
carbon tetrachloride	2.197094933	3.225891753	3.743303059
SRF	2.875763712	3.021940988	3.047740719
APP	2.213211487	2.719834122	3.925550359
decitabine	2.683281573	2.451851649	3.386959923
SMAD3	2.52504777	2.446393305	3.53403947
Akt	2	2.906721392	3.510076044
TGFB3	2.128608337	2.771182334	3.243389606
MKL1	2.413168869	2.942860456	2.392525135
lysophosphatidic acid	2.200431147	2.418763848	2.771834041
ERBB2	2.311681967	2.085470535	2.153617844
<hr/>			
Predicted Upstream Regulators of AP - CD9 ⁺ Gene Expression Profile			
Upstream regulators	Relative to CD29 ^{Low}	Relative to CD29 ^{High}	Relative to AP - CD9 ⁺
dexamethasone	3.723585844	3.418205705	2.455115621
dihydrotestosterone	3.040095564	3.324915908	2.182751614
ESR1	4.032211281	2.347165401	2.449489743
IL1B	6.942948833	8.014142705	2.275259404
IL22	3.696418146	3.696418146	2.218800785
IL6	5.614511061	6.583471321	2.54701974
lipopolysaccharide	8.256984447	9.563856334	3.68065562
NFkB (complex)	6.635890037	7.305010563	2
OSM	5.104536818	5.767256949	2.373267208
STAT3	4.04276135	4.173063327	2.19089023
TNF	6.05482009	7.622307827	3.51255496
<hr/>			
Predicted Upstream Regulators of AP - CD9 ⁺ Gene Expression Profile			
Upstream regulators	Relative to CD29 ^{Low}	Relative to CD29 ^{High}	Relative to AP - CD9 ⁻
lipopolysaccharide	7.463103237	8.763766185	2.055045068
IFNG	5.59492072	6.329520291	2.928682494
phorbol myristate acetate	6.260259793	6.312984518	2.143015537
TGFB1	5.062175745	4.97882322	2.736808601

bleomycin	3.785675976	4.013372103	2.161290323
Predicted Upstream Regulators of CD29^{Low} Gene Expression Profile			
Upstream regulators	Relative to CD29 ^{High}	Relative to AP - CD9 ⁺	Relative to AP - CD9 ⁻
lipopolysaccharide	8.128169042	7.350060458	7.718544044
TNF	7.578688129	7.134880242	7.884864732
IFNG	7.035556616	6.384884443	6.669484393
phorbol myristate acetate	6.479213594	6.598866455	6.954527633
CSF2	5.96689163	5.846197862	6.129084236
poly rI:rC-RNA	6.032696025	5.972792155	5.906591149
E. coli B4			
lipopolysaccharide	5.787355652	5.78676962	5.795720503
tretinoin	5.790432476	5.379575495	5.676848653
NFKB (complex)	6.102638949	5.32626923	5.408527935
IL1B	5.816582183	5.197506626	5.421027382
hydrogen peroxide	5.000113091	5.630983681	5.635967762
TGM2	5.166046678	5.249198959	5.148718313
IL6	5.214965709	4.874859377	5.032833974
salmonella minnesota R595			
lipopolysaccharides	5.005666928	5.100990241	4.902447123
E. coli B5			
lipopolysaccharide	4.818599685	5.225535987	4.923232242
cardiotoxin	4.795831523	5.196152423	4.898979486
bleomycin	4.55412042	4.852073819	5.222371255
MYD88	4.959531596	4.677162706	4.836953626
TGFB1	3.86063439	5.25819459	5.353843236
trinitrobenzenesulfonic acid	4.885140105	4.691479128	4.783188537
AGT	4.50010328	4.771588744	4.931342505
SMARCA4	4.387461609	4.660797343	5.112244322
IL1	5.092437492	4.526204044	4.526204044
Salmonella enterica serotype			
abortus equi			
lipopolysaccharide	4.204809747	4.443556268	4.871379382
CpG oligonucleotide	4.61823895	4.616554627	4.283983617
IL1A	4.76509979	4.253272398	4.453261807
IL5	4.232041843	4.449286195	4.746519792
CEBPA	4.346381509	4.670108601	4.389377142
IL2	4.941072607	4.087132846	4.337701077
TNFSF12	4.462033792	4.371886999	4.371886999
palmitic acid	4.369417335	4.361956415	4.46725786
PI3K (complex)	4.423942768	4.545582054	4.216192975
TICAM1	4.438730068	4.335454162	3.991281203
IKBKB	4.919466494	3.920704637	3.850832618
EGF	3.712911953	4.129517483	4.816909494

TLR4	4.831282043	3.558789315	4.152221192
RELA	4.122540707	4.020808224	4.269009529
deferoxamine	3.414440248	4.263717025	4.600787692
CEBPB	4.847688618	3.875001276	3.498038982
CSF1	3.500698217	4.49340543	4.178205498
EGR1	4.261952838	3.775610639	4.027663178
RAF1	3.533282166	4.061901976	4.408530809
TLR3	4.504826084	3.788357216	3.686995716
P38 MAPK	3.993399107	3.855003662	4.089391765
lipid A	4.050851069	3.926063953	3.926063953
TLR7	3.906598046	4.023946573	3.897950939
SPI1	3.616445651	4.087219419	3.982750352
MAPK14	3.490175848	4.011936423	4.113382077
CHUK	4.516256144	3.419734831	3.670672206
ERK1/2	3.461852363	3.810775377	4.311716354
RETNLB	3.605551275	3.860234248	4.110960958
5-O-mycetyl-beta-araf-(1->2)-5-O-mycetyl-alpha-araf-(1->1')-glycerol	3.83349086	3.741657387	4
STAT4	3.916376069	3.802145728	3.810847422
CpG ODN 1826	3.903371495	3.791840265	3.791840265
SIM1	4	3.741657387	3.741657387
ARNT2	4	3.741657387	3.741657387
phytohemagglutinin	3.597519018	3.574726541	4.292721525
Akt	3.420246105	3.957705466	4.042084274
Vegf	3.069687124	4.108975725	4.200373621
Interferon alpha	3.840654406	3.798302276	3.581867509
MAP2K1	3.11713043	4.048936507	4.039380684
AKT1	3.481943753	3.841927386	3.84741875
MAP3K8	3.491794935	3.768329836	3.890164827
resiquimod	3.610018557	3.721566706	3.797775309
cisplatin	3.599288885	4.162860104	3.363552711
LDL	4.195145568	3.395304585	3.529284947
F2	3.459084314	3.785413637	3.689119285
APP	4.117696816	3.448687516	3.367105544
thapsigargin	3.907090936	3.364772005	3.640078408
hemozoin	3.623304079	3.626026329	3.626026329
carbon tetrachloride	3.528039522	3.389397373	3.910355733
E. coli serotype 0127B8 lipopolysaccharide	3.589776549	3.177061192	4.014243371
TLR9	3.903140171	3.413193006	3.387474376
TNFSF11	3.177105232	3.671647272	3.78721576
CSF3	3.12637894	3.372466041	4.086616852

ethanol	2.988686091	3.72912958	3.851435131
IL21	3.571987831	3.836783592	3.134399467
FN1	3.536269528	3.550289405	3.439021298
EDN1	3.189076046	3.324767734	4.00491243
D-glucose	2.538384476	3.890039536	4.035840521
enterotoxin B	3.6476299	3.512484023	3.22706429
STAT1	4.130709991	3.036433428	3.219145306
ERK	3.192690978	3.427836275	3.680543596
IL4	3.001280201	3.601330244	3.666562155
PDGF BB	4.256975939	2.805364178	3.121015544
HGF	3.400603265	3.218611598	3.527842383
IL18	3.717176793	3.061529524	3.346563096
peptidoglycan	3.537895007	3.266804662	3.311649761
MGEA5	4.428858317	2.591193878	3.088201143
FOXO1	2.749339057	3.356394556	3.987603016
lipoteichoic acid	3.158467599	3.402841303	3.528730696
PRKCD	3.082187546	3.341500125	3.624969804
Pkc(s)	2.785677255	3.635469908	3.604173826
vancomycin	3.421869846	3.278475385	3.278475385
SP1	2.974179613	2.91930169	4.053027903
GATA2	3.837013861	3.190779947	2.892630476
Ap1	3.107914288	3.250954965	3.540515513
Tlr	3.356045823	3.342794529	3.190571833
Creb	3.294421195	3.217811238	3.358035373
MALP-2s	3.376000773	3.225376815	3.225376815
IL17A	3.437835542	3.448551157	2.931644304
CD40LG	3.131955453	3.269745228	3.411764818
Jnk	3.202876482	3.361531012	3.23184661
KRT17	3.16227766	3.31662479	3.31662479
aldosterone	3.395068348	3.108536206	3.265421955
CXCL12	2.796439786	3.226400341	3.649495786
PLG	3.416568759	3.116712797	3.116712797
cholesterol	3.29672351	2.981775781	3.368493296
PTGER2	3.124431314	3.254450989	3.254450989
Pam3-Cys	3.011987158	3.295742977	3.295742977
ITK	3.137858162	3.292523039	3.137858162
CREB1	3.880829371	2.7944332	2.887004032
lysophosphatidic acid	3.071379917	3.248709431	3.232287779
Ca2+	3.636084506	3.048512801	2.807541319
IL12 (complex)	3.616924595	2.864846103	2.920178104
thioacetamide	2.719600415	3.267533383	3.412320069

kainic acid	3.049971773	3.012912766	3.321392616
OSM	3.464231322	3.13406463	2.75760041
tunicamycin	2.850632328	3.056539329	3.35870494
EP300	3.345212363	3.036881419	2.882572444
CCL5	2.690824936	3.270950116	3.270950116
HIF1A	3.084955388	2.87955057	3.262468243
N-acetyl muramyl-L-alanyl-D-isoglutamine	3.070086966	2.92626065	3.211536046
TET2	3	2.886751346	3.31662479
IL15	3.085621557	2.54833386	3.544137042
E. coli lipopolysaccharide	3.01466967	2.993256178	3.126878886
JUN	3.249727121	2.9348216	2.9348216
hexachlorobenzene	2.812719752	3.147573112	3.147573112
cigarette smoke	3.544091603	2.543258445	3.017215195
uric acid	2.932356088	3.002634328	3.137841465
1-methyl-4-phenyl-1,2,3,6-tetrahydropyridine	3.0697565	3.057412207	2.907733474
NOD2	2.96147567	2.790259827	3.278230315
TREM1	2.628980905	2.969926118	3.407952274
gentamicin C	2.984810029	3	3
KITLG	3.241142923	2.963445212	2.754102208
IL27	2.69894894	3.035844207	3.192518941
triamterene	2.969261484	2.970442629	2.970442629
NOS2	3.227550383	2.685804157	2.985046469
ionomycin	2.471118258	3.125986024	3.262298148
forskolin	3.159589076	2.700619564	2.99561059
GATA1	2.740500835	3.054715755	3.054715755
ETS2	3.09815346	2.961125118	2.789473684
SELPLG	2.828427125	2.828427125	3.16227766
S100A9	2.39616166	3.059388806	3.35557883
HRG	2.645751311	3.16227766	3
IL3	2.295276167	2.820440962	3.683003683
decitabine	2.686312031	2.393494007	3.704647478
Fcer1	2.67845935	2.967258717	3.130706929
Hbb-b2	2.449489743	3.16227766	3.16227766
CAMP	2.904012696	2.694819842	3.162377346
IFN alpha/beta	3.328201177	2.722178615	2.703465338
PTGS2	3.060727345	3.061014129	2.602129977
LEP	2.807418382	3.2458771	2.655525899
acetaminophen	2.746743679	3.101282295	2.833513717
C5AR1	2.78941699	2.939498828	2.939498828
PLAUR	2.607090922	3.098694041	2.958934625

PRKCA	3.108757041	2.77944719	2.769666046
deferasirox	2.828427125	2.828427125	3
trichostatin A	2.934704543	2.694491869	2.971003422
IL13	3.347276302	2.362765129	2.878790385
Collagen type I	2.812719752	2.803652103	2.970442629
GLI1	2.187409922	2.902603708	3.496254199
KLF4	2.634373184	2.875882702	3.039452717
HMGB1	3.057040622	2.742667774	2.742667774
Cg	3.21876573	3.017181638	2.303651471
TAC1	2.894340641	2.732690729	2.894340641
IRF7	2.756122108	2.758386422	3
mir-223	2.553616667	2.453738644	3.478505426
SAMSN1	3	2.828427125	2.645751311
TFEB	2.201280896	3.12533359	3.135019371
TP53	2.280606696	2.904428022	3.257869917
gentamicin	2.516611478	3.242933289	2.679975002
5-hydroxytryptamine	2.756100307	2.752782077	2.920835173
F3	2.58613097	3	2.828427125
NFKB1	2.991309016	2.704245572	2.704245572
CpG ODN 1668	2.955914411	2.627079213	2.809948949
SAA1	2.796315261	2.796315261	2.796315261
Pam3-Cys-Ser-Lys4	3.598417453	2.566845507	2.201954168
MAPK7	2.951529242	2.61280915	2.796868233
zymosan	2.985083116	2.813364212	2.557043578
TYROBP	2.726050089	2.726050089	2.898360588
TLR2	3.638204313	2.619819133	2.089750887
C5	2.782350117	2.782350117	2.782350117
doxorubicin	2.734869407	2.707536655	2.868552674
DOCK8	2.828427125	2.828427125	2.645751311
AR	2.201127266	3.196752393	2.902092148
CCL11	2.934057882	2.587986557	2.770141551
HRAS	2.916081581	2.864357773	2.497916566
reactive oxygen species	2.899503735	2.580219806	2.763800826
D-fructose	2.433567753	2.811998561	2.98449602
2-bromoethylamine	2.975337221	2.621093259	2.621093259
MET	3.147573112	2.34520788	2.719600415
tributyrin	2.949563804	2.621093259	2.621093259
SMARCB1	2.812719752	2.596174831	2.778433094
IKBKG	3.167574316	2.50556587	2.50556587
IRF8	2.807026118	2.661006678	2.710270376
imiquimod	2.783758531	2.439502069	2.934571435

NFKBIA	2.866954016	2.432527631	2.849344661
CYP2E1	2.775190801	2.589619002	2.775190801
fenamic acid	2.593838854	2.562726589	2.970442629
hyaluronic acid	2.608610252	2.715476433	2.798423093
HTT	2.050777725	3.111269837	2.948839123
CEBPD	2.973499842	2.475718832	2.641610685
ECSIT	2.576836178	2.574409875	2.931419509
trovafloxacin	2.538365413	2.984810029	2.538365413
alitretinoin	2.94073308	2.744433483	2.370289241
VEGFA	3.174500159	2.546369382	2.30284445
CD44	2.961306692	2.883685925	2.169665245
ETS1	2.490434364	3.039624493	2.447516471
PI3K (family)	2.734678727	2.858820058	2.362000571
Brd4	2.449489743	2.828427125	2.645751311
cyclic AMP	2.138858779	2.969461529	2.795134702
cholecalciferol	2.391902755	2.662206876	2.83986673
MTPN	2.645751311	2.432700719	2.799769576
leukotriene D4	2.746779251	2.373220598	2.753479958
ITGB1	2.104447187	2.718093592	3.040494833
10E,12Z-octadecadienoic acid	2.464707482	2.608006848	2.788610696
fatty acid	2.349177285	2.5899612	2.917948757
CD14	2.80308074	2.421686614	2.602236228
dextran sulfate	2.90200169	2.423104362	2.423104362
lomustine	2.449489743	2.645751311	2.645751311
A23187	2.962134655	2.378142769	2.378142769
RAC1	2.788610696	2.653613888	2.275801333
FFAR3	2.333333333	3	2.333333333
PTPRJ	3	2.333333333	2.333333333
CTNNB1	2.031471352	2.828788223	2.795725562
CXCL3	2.606524477	2.606524477	2.417706324
RUNX1	2.083691952	2.78107851	2.764378962
MAPK8	3.024999129	2.560167892	2.024553943
cytarabine	2.787161141	2.407572883	2.407572883
methamphetamine	2.415120612	2.591465305	2.591465305
CD38	2.34520788	2.618614683	2.618614683
sodium chloride	2.216481463	2.414184025	2.941922949
LAMA5	2.392050778	2.580114742	2.580114742
TLR5	2.758778666	2.385210844	2.385210844
NFATC2	2.502262382	2.473029162	2.473029162
MAP2K1/2	2.184260142	2.550115269	2.704006629

IRAK4	2.343166873	2.547327476	2.547327476
Nfat (family)	2.932975147	2.13459255	2.338738329
JAK2	2.895660922	2.428105047	2.069450136
CXCL2	2.592082948	2.395108329	2.395108329
TNNI3	2.449489743	2.449489743	2.449489743
bromodeoxyuridine	2.449489743	2.449489743	2.449489743
SASH1	2.645751311	2.449489743	2.236067977
cyclooxygenase	2.449489743	2.432700719	2.432700719
SAA	2.570447573	2.369115447	2.369115447
TNFSF14	2.225082386	2.438546298	2.635605319
D-galactosamine	2.191117266	2.363290446	2.736617642
IL17C	2.422507916	2.422507916	2.422507916
MAP3K1	2.416190854	2.423170827	2.423170827
RIPK2	2.47309379	2.275652605	2.49878147
monophosphoryl lipid A	2.414246417	2.414246417	2.414246417
ICAM1	2.205501537	2.421341943	2.58785544
bee venom	2.631006803	2.222839083	2.349330283
Ccl2	2.797899809	2.271982002	2.090613582
PLAU	2.399617745	2.490761275	2.255610596
chrysotile asbestos	2.578947368	2.176470588	2.385210844
ethionine	2.236067977	2.449489743	2.449489743
triclosan	2.236067977	2.449489743	2.449489743
REL	2.574991625	2.180543583	2.370094641
BCR (complex)	2.672962916	2.302648852	2.109284469
IL11RA	2.432700719	2.218800785	2.42535625
Tnf (family)	2.46766482	2.07902851	2.519811939
lysophosphatidylcholine	2.213211487	2.406820311	2.406820311
cobalt chloride	2.591465305	2.202095354	2.202095354
ITGA5	2.200431147	2.395108329	2.395108329
Pka	2.111111111	2.299985027	2.503056989
C5	2.30282306	2.440591355	2.165286233
ozone	2.169304578	2.363636364	2.363636364
CXCL8	2.379855129	2.150772103	2.35301929
CSF1R	2.156655464	2.35975021	2.35975021
GC-GCR dimer	2.218800785	2.218800785	2.432700719
FOXL2	2.437995124	2.215646838	2.215646838
3M-001	2.422718559	2.218632484	2.218632484
CD2	2.343418378	2.367588444	2.146625258
CYBB	2.359071298	2.359071298	2.137186835
C3	2.138474401	2.435002935	2.2681532
Mapk	2.400626681	2.200431147	2.200431147

TCR	2.22697724	2.194988511	2.352630912
CD36	2.385210844	2.176470588	2.176470588
stallimycin	2.236067977	2.236067977	2.236067977
N(2)-(gamma-D-glutamyl)-meso-2,2'-diaminopimelic acid	2.218800785	2.236067977	2.236067977
IFNGR1	2.228344058	2.228344058	2.228344058
phenylbutazone	2.223493925	2.223781797	2.223781797
IL17a dimer	2.215395102	2.215395102	2.215395102
MOG	2.153205645	2.153205645	2.322630901
TLR8	2.208069705	2.208069705	2.208069705
PTGES	2.2	2.186432666	2.186432666
CYR61	2.197492626	2.185934949	2.185934949
CEBPE	2.047954809	2.230597631	2.230597631
KLK5	2.449489743	2	2
methyl methanesulfonate	2.163657997	2	2.2
IL17RA	2.098366355	2.098366355	2.098366355
APCS	2.236067977	2	2
urethane	2.186432666	2	2
CTSZ	2	2	2
IL-17f dimer	2	2	2
8-hydroxyguanine	2	2	2
ABCC1	2	2	2

Table S3. Mouse primers used for gene expression analysis.

Gene	Forward primer (5'-3')	Reverse primer (5'-3')
<i>Ackr2</i>	AGTCTGGCTCTGCCTGTTCTG	CCTCGCTTGCAGAGTTGTGG
<i>Acp5</i>	AGAACGGTGTGGCTATGTG	GGACCTTCGTTGATGTCGC
<i>Acta2</i>	GTCGGCAGACATCAGGGAGTAA	TCGGATACTTCAGCGTCAGGA
<i>Actb</i>	ATCAAGATCATTGCTCCCTGAG	CTGCTTGCTGATCCACATCTG
<i>Adamts4</i>	GAGTCCCATTCCCCGAGAA	ATAACCCTCAGCAGGTAGCG
<i>Adipoq</i>	CACACCAGGCCGTATGGCA	CAGTGACGCCGGTCTCCAGC
<i>Ald1</i>	GGAAAGAGCATCCGTACCGT	GTTCAGAAACTGGTGCCTGG
<i>Adam12</i>	GCTCCACCCTCTGTGACAA	TCCTACAGTCAAGCCCTGGT
<i>Bmp2</i>	TTCCATCACGAAGAAGCCGT	GAAACTCGTCACTGGGACA
<i>Bmp7</i>	ACGCCACCAACCACGCCATC	GTGTGGCCCCGCAAAGGTCA
<i>Cebpa</i>	CCCAGAGGACCAATGAAATGAAG	TAGCCGGAGGAAGCTAAGAC
<i>Cbr2</i>	GGAAAGGGATTGGACGGGAC	CACACACGGGCTCTATTCCG
<i>Ccl2</i>	TTAAAAAACCTGGATCGAACCAA	GCATTAGCTTCAGATTTACGGGT
<i>Ccl6</i>	TTCGCCCTGCCACAATAGAG	ATTTCACCCCAAGAGGCCAG
<i>Ccl7</i>	CCATCAGAAGTGGGTCGAGG	TGCTTCTGGCTCCTAGGTTG
<i>Ccl8</i>	CTGAAGATCCCCCTTCGGGT	CCCACTCTGTGTGGGTC
<i>Ccl11</i>	AGCTAGTCGGAGAGCCTAC	AAGGAAGTGACCGTGAGCAG
<i>Ccl17</i>	CCACCAATGTAGGCCGAGAG	ATGGCATCCCTGGAACACTC
<i>Ccl22</i>	TTGGCCTCCACCTACTCTCA	CGTGCTGCAGACCAAGAAC
<i>Ccr7</i>	AGGGAAACCCAGGAAAAACGTG	GACCTCATCTTGGCAGAAGCA
<i>Cd34</i>	CTGGAATCCGAGAAGTGAGGTTGG	AGTTTGCTGGGAATTCTGTGCTATTG
<i>Cd209a</i>	GGGGCTCAACTTGTGGTCAT	GAGCCCCATCCAAGTGTAGC
<i>Colla1</i>	ACGTCCTGGTGAAGTTGGTC	TCCAGCAATACCCCTGAGGTC
<i>Col3a1</i>	CTGGTCCTGTTGGTCCATCT	ACCTTTGTCACCTCGTGGAC
<i>Coll2a1</i>	GCTATCCAGGTTCCGGCTAA	CCCTCCTGTATGATGCCGAC
<i>Cilp</i>	CTGCCTGCCTTCTGTGATGA	CTGAGGGACACCGATTGCAT
<i>Ctgf</i>	AGCCGCCTCTGCATGGTCA	GCGATTAGGTGTCCGGAT
<i>Cxcl1</i>	AACACAAGATCCGGCAGAGG	ACGGCTAGGAAAGGGTCTCT
<i>Cxcl2</i>	CCAACCACCAGGCTACAGG	GCGTCACACTCAAGCTCTG
<i>Cxcl4</i>	CAGTGGCACCCCTTGTGACAT	ATCGCTTCTTCGGGACAG
<i>Cxcl12</i>	AACACAAGATCCGGCAGAGG	ACGGCTAGGAAAGGGTCTCT
<i>Cxcl14</i>	GTCACCGAGTGGTTCTGCAT	TTCAAGCACGCCCTCTCTG
<i>Desmin</i>	AGGGCGAGGAGAGCAGGATCAACC	CGCTGACAACCTCTCCATCCG
<i>Dpp4</i>	CCAGCAGTGCCTCTCCTTACA	GGGGACAGGCATCCTTAGTT
<i>Edn1</i>	CGGGTCTTATCTCTGGCTGC	AGTTCTCCGCCGCCCTTTTA
<i>Egr1</i>	TGCGGCCATCTCTCCCTCCTGT	CCATCCCCCTGCCACCACCTCATT
<i>Egr2</i>	TTCGGCAGAAGGAACCGAACAGCAG	ATGGGGAGGAACAGGAAGGGTGGTG
<i>Egr3</i>	GGCGCACCCCTTCTCGACTTCT	AGCCGCAGCGACCACCTCACCAC
<i>Fgf9</i>	ACGGTCGGATGGATGAAGA	TGGCACAGGTTCAAGGTCAA
<i>Fn</i>	CTACCCCTGCAGCCTCTGCGC	TCACCTCCCTGGCTCGGTG
<i>Gas6</i>	ATGAAGATCGCGTAGCTGG	CCAACCTCCATGCACCCAT
<i>Gpr34</i>	CTGCCTCCCTTCCGCATAA	TGCTTGGTGGTTATTGCCCT
<i>Grasp</i>	CCCTAACACCATCAAGCAGAGAG	TGCAGCTCCTGAGTCGGC
<i>Hmox1</i>	GAACCCAGTCTATGCCAAC	GGCGTGCAAGGGATGATTTC
<i>Igf1</i>	GCCCAAGACTCAGAACGGCC	TGCAGGTTGCTCAAGCAGCA
<i>Igf2</i>	GCCTCGTCACCTCTCCTACG	CAGTGTCCAGTGCCTGTTG
<i>Il1a</i>	TTGGTTAAATGACCTGCAACA	GAGCGCTCACGAACAGTTG
<i>Il1b</i>	TTGACGGACCCAAAAGAT	GAAGCTGGATGCTCTCATCTG
<i>Il1rl1</i>	ATGACTGTCTGGCCCTGAAC	AGCAATGTGTGAGGGACACT

<i>Il6</i>	ACCGCTATGAAGTTCCCTCTGCAA	TGCAGGTTGCTCAAGCAGCA
<i>Il12b</i>	AAGAGCAGTAGCAGTCCCC	GTTGGGCAGGTGACATCCTC
<i>Il31ra</i>	CAGCCTGGACTTCCCAGATA	GCTTGACTTCCAAGAGCCG
<i>Il33</i>	CACATTGAGCATCCAAGGAA	AACAGATTGGTCATTGTATGTACTCAG
<i>Il36g</i>	CCTCCCATGCAACTACCCAG	GCTCAGGGTGGTGGTACAAA
<i>Irf4</i>	TCCCACGGACACACCTATGA	GTCCATTGTCGTCCGGTAG
<i>Itgam</i>	TTCCTGGTGCCAGAAGCTGAA	CCCGTTGGTCGAACTCAGGA
<i>Klf4</i>	CCGGCGGGAAAGGGAGAACACT	CGCCGGGAAGACGGAGGATGAA
<i>Lyve1</i>	CCAAAACACTACGGTGCATGC	GGCATGAAACTTGCCTCGTG
<i>Maf</i>	AAGGGACGCCTACAAGGAGA	GAGAGGAAGGGTTGTCGCTG
<i>Mgl2</i>	GAUTGAGTTCTCGCCTCTGG	CTGGGAAGGAATTAGAGCAAAC
<i>Mgll</i>	TGCTCGGGGAACGTGACA	ACTGTCCTGCTGCATTGACC
<i>Mif1</i>	CGGCAAGCCGCACAGTACATC	CACGTTGGCAGCGTT CAT
<i>Mmp2</i>	CTTCGCTCGTTCCCTCAAC	ATGTCAGACAACCCGAGTCC
<i>Mmp9</i>	ATCCCCAGAGCGTCATTGCG	CACGTAGCCCACGTCGTCCAC
<i>Mmp12</i>	CCACGCGTCCGTTGATGAG	CTGTCATTCATGGGAGCAGCC
<i>Mmp13</i>	GACCCCAACCTTAAGCATCC	CCTCGGAGACTGGTAATGGC
<i>Mmp14</i>	TTCGTGTTGCCTGATGACGA	TTCCCGTCACAGATGTTGGG
<i>Mrc1</i>	CAAGGAAGGTTGGCATTGT	CCTTCAGTCCTTGCAAGC
<i>P2ry10</i>	GAGGTAATCCAGGATATGTGCTTGC	AATTATGGCCCCCTGATGCT
<i>Pcolce2</i>	AGTGGCTTCATGGCAACGTA	CCGGAAGGTTTTCAAGGCG
<i>Pdgfa</i>	CGCTGCACTGGCTTGTAA	GCCGGCTCATCTCCACCTCA
<i>Pdgfc</i>	GGAACAGAACGGAGTGCAAGA	TGAGGAAACTCAGGCTGTG
<i>Plin1</i>	GACACCACCTGCATGGCT	TGAAGCAGGGCCACTCTC
<i>Pparg2</i>	TTCGCTGATGCACTGCCTATGAG	ACAGAGCTATTCCGAAGTTGGT
<i>Ramp3</i>	GCTGCTTGTGGTGAGTGTG	ACACGATGAACCTCCGACAGG
<i>Relma</i>	CCCAGGATGCCAACTTGAA	GGCCCATCTGTTCATAGTCT
<i>S100a8</i>	AAATCACCATGCCCTCTACAAG	CCCACTTTATCACCATCGCAA
<i>S100a9</i>	ATACTCTAGGAAGGAAGGACACC	TCCATGATGTCATTATGAGGGC
<i>Siglec1</i>	CTGCTCTGTACAACTCAGGT	AAGAGGCTTGGAAAGGCAAGTC
<i>Tgfb1</i>	ACGCCTGAGTGGCTGTCTTGAC	GGGCTGATCCCGTTGATTCCACG
<i>Timp1</i>	TCCCCAGAAATCAACGAGACC	GGGCATATCCACAGAGGCTT
<i>Tlr4</i>	TGGCTGGTTACACGTCCAT	TGCAGAAACATTGCCAAGC
<i>Tlr8</i>	ATGCCAACAAACAGCACCCA	GGCAACCCAGCAGGTATAGT
<i>Tnc</i>	GGAGCCAGGGCAAGAATACA	ATGGCCGTGGATGCCTTC
<i>Tnfaip6</i>	GCTCACGGATGGGGATCAA	TTGTAGGTTGCGAGACGACC
<i>Tnn</i>	CCTTCCCCCTGGGATTCTG	TCATCGCTGAGTGACTGTGG
<i>Txnip</i>	CAGTCTCTACAGCGGGGAAAC	GGAGACCCGCCTACTGATTG
<i>Vegfa</i>	CGACACGGGAGACAATGGGATGAA	AGGGGGCGGGGTGCTTTGTAGACT
<i>Wnt5a</i>	TCAAGGAATGCCAGTACCACTTC	CTGTTGACCTGCACCAGCTT
<i>Wnt11</i>	AAGAAGCTATCCTCGCCGCT	GTGGATAGGGAGAGTGCAGGA

References and Notes:

1. T. A. Wynn, K. M. Vannella, Macrophages in Tissue Repair, Regeneration, and Fibrosis. *Immunity*. **44**, 450–462 (2016).
2. S. Ebmeier, V. Horsley, Origin of fibrosing cells in systemic sclerosis. *Current Opinion in Rheumatology*. **27**, 555–562 (2015).

3. A. Gosain, L. A. DiPietro, Aging and wound healing. *World J Surg.* **28**, 321–326 (2004).
4. C. B. Ballas, J. M. Davidson, Delayed wound healing in aged rats is associated with increased collagen gel remodeling and contraction by skin fibroblasts, not with differences in apoptotic or myofibroblast cell populations. *Wound Repair Regen.* **9**, 223–237 (2001).
5. T. Fujiwara *et al.*, Age-Associated Intracellular Superoxide Dismutase Deficiency Potentiates Dermal Fibroblast Dysfunction During Wound Healing. *Exp. Dermatol.* (2017), doi:10.1111/exd.13404.
6. N. Vedrenne, B. Coulomb, A. Danigo, F. Bonté, A. Desmoulière, The complex dialogue between (myo)fibroblasts and the extracellular matrix during skin repair processes and ageing. *Pathologie Biologie.* **60**, 20–27 (2012).
7. E. C. Naylor, R. E. B. Watson, M. J. Sherratt, Molecular aspects of skin ageing. *Maturitas.* **69**, 249–256 (2011).
8. E. Kohl, J. Steinbauer, M. Landthaler, R. M. Szeimies, Skin ageing. *Journal of the European Academy of Dermatology and Venereology.* **25**, 873–884 (2011).
9. T. Tabib, C. Morse, T. Wang, W. Chen, R. Lafyatis, SFRP2/DPP4 and FMO1/LSP1 Define Major Fibroblast Populations in Human Skin. *Journal of Investigative Dermatology.* **138**, 802–810 (2018).
10. C. Philippeos *et al.*, Spatial and Single-Cell Transcriptional Profiling Identifies Functionally Distinct Human Dermal Fibroblast Subpopulations. *Journal of Investigative Dermatology.* **138**, 811–825 (2018).
11. R. R. Driskell, F. M. Watt, Understanding fibroblast heterogeneity in the skin. *Trends in Cell Biology.* **25**, 92–99 (2015).
12. J. M. Sorrell, Fibroblast heterogeneity: more than skin deep. *Journal of Cell Biology.* **117**, 667–675 (2004).
13. R. G. Marangoni *et al.*, Myofibroblasts in murine cutaneous fibrosis originate from adiponectin-positive intradermal progenitors. *Arthritis Rheumatol.* **67**, 1062–1073 (2015).
14. Y. Rinkevich *et al.*, Identification and isolation of a dermal lineage with intrinsic fibrogenic potential. *Science.* **348**, aaa2151–aaa2151 (2015).
15. R. R. Driskell *et al.*, Distinct fibroblast lineages determine dermal architecture in skin development and repair. *Nature.* **504**, 277–281 (2013).
16. D. Jiang *et al.*, Two succeeding fibroblastic lineages drive dermal development and the transition from regeneration to scarring. *Nat Cell Biol.* 1–19 (2018).
17. I. A. Darby, B. Laverdet, F. Bonté, A. Desmoulière, Fibroblasts and myofibroblasts in wound healing. *CCID*, 301 (2014).
18. B. Hinz *et al.*, Recent Developments in Myofibroblast Biology. *AJPA.* **180**, 1340–1355 (2012).
19. T. A. Wynn, T. R. Ramalingam, Mechanisms of fibrosis: therapeutic translation for fibrotic disease. *Nat Med.* **18**, 1028–1040 (2012).
20. M. V. Plikus *et al.*, Regeneration of fat cells from myofibroblasts during wound healing. *Science*,

aai8792 (2017).

21. T. Iwayama *et al.*, PDGFR α signaling drives adipose tissue fibrosis by targeting progenitor cell plasticity. *Genes Dev.* **29**, 1106–1119 (2015).
22. G. Marcellin *et al.*, A PDGFR α -Mediated Switch toward CD9(high) Adipocyte Progenitors Controls Obesity-Induced Adipose Tissue Fibrosis. *Cell Metabolism*. **25**, 673–685 (2017).
23. R. Higashiyama *et al.*, Differential Contribution of Dermal Resident and Bone Marrow-Derived Cells to Collagen Production during Wound Healing and Fibrogenesis in Mice. *J. Invest. Dermatol.* **131**, 529–536 (2011).
24. O. Kanisicak *et al.*, Genetic lineage tracing defines myofibroblast origin and function in the injured heart. *Nature Communications*. **7**, 1–14 (2016).
25. R. Berry, M. S. Rodeheffer, Characterization of the adipocyte cellular lineage in vivo. *Nat Cell Biol.* **15**, 302–308 (2013).
26. G. C. Rivera-Gonzalez *et al.*, Skin Adipocyte Stem Cell Self-Renewal Is Regulated by a PDGFA/AKT-Signaling Axis. *Stem Cell*. **19**, 1–25 (2016).
27. C. D. Church, R. Berry, M. S. Rodeheffer, Isolation and study of adipocyte precursors. *Meth. Enzymol.* **537**, 31–46 (2014).
28. M. S. Rodeheffer, K. Birsoy, J. M. Friedman, Identification of white adipocyte progenitor cells in vivo. *Cell*. **135**, 240–249 (2008).
29. B. M. Lichtenberger, M. Mastrogiovanni, F. M. Watt, -catenin activation remodels the dermis via paracrine signalling to distinct fibroblast lineages. *Nature Communications*. **7**, 1–13 (2016).
30. T. Ostendorf, F. Eitner, J. Floege, The PDGF family in renal fibrosis. *Pediatr. Nephrol.* **27**, 1041–1050 (2011).
31. L. J. Reigstad, J. E. Varhaug, J. R. Lillehaug, Structural and functional specificities of PDGF-C and PDGF-D, the novel members of the platelet-derived growth factors family. *FEBS J.* **272**, 5723–5741 (2005).
32. J. C. Bonner, Regulation of PDGF and its receptors in fibrotic diseases. *Cytokine & Growth Factor Reviews*. **15**, 255–273 (2004).
33. S. Dulauroy, S. E. Di Carlo, F. Langa, G. E. R. Eberl, L. Peduto, Lineage tracing and genetic ablation of ADAM12+ perivascular cells identify a major source of profibrotic cells during acute tissue injury. *Nat Med.* **18**, 1262–1270 (2012).
34. S. Paquet-Fifield *et al.*, A role for pericytes as microenvironmental regulators of human skin tissue regeneration. *Journal of Clinical Investigation*, 1–12 (2009).
35. S. Werner, R. Grose, Regulation of wound healing by growth factors and cytokines. *Physiol. Rev.* **83**, 835–870 (2003).
36. J. Ding, E. E. Tredget, The Role of Chemokines in Fibrotic Wound Healing. *Advances in Wound Care*. **4**, 673–686 (2015).
37. M. Xue, C. J. Jackson, Extracellular Matrix Reorganization During Wound Healing and Its Impact on Abnormal Scarring. *Advances in Wound Care*. **4**, 119–136 (2015).

38. I. Goren *et al.*, A Transgenic Mouse Model of Inducible Macrophage Depletion. *AJPA*. **175**, 132–147 (2010).
39. T. Lucas *et al.*, Differential Roles of Macrophages in Diverse Phases of Skin Repair. *Journal of Immunology (Baltimore, Md. : 1950)*. **184**, 3964–3977 (2010).
40. R. Mirza, L. A. DiPietro, T. J. Koh, Selective and Specific Macrophage Ablation Is Detrimental to Wound Healing in Mice. *AJPA*. **175**, 2454–2462 (2010).
41. B. Shook, E. Xiao, Y. Kumamoto, A. Iwasaki, V. Horsley, CD301b+ Macrophages Are Essential for Effective Skin Wound Healing. *J. Invest. Dermatol.* **136**, 1885–1891 (2016).
42. C. B, C. Burkhardt, W. Reith, R. Renkawitz, I. Forster, Conditional gene targeting in macrophages and granulocytes using LysMere mice. *Transgenic research*. **8**, 265–277 (1999).
43. T. Buch *et al.*, A Cre-inducible diphtheria toxin receptor mediates cell lineage ablation after toxin administration. *Nature Publishing Group*. **2**, 419–426 (2005).
44. J. M. Daley, S. K. Brancato, A. A. Thomay, J. S. Reichner, J. E. Albina, The phenotype of murine wound macrophages. *Journal of Leukocyte Biology*. **87**, 59–67 (2010).
45. R. Mirza, T. J. Koh, Dysregulation of monocyte/macrophage phenotype in wounds of diabetic mice. *Cytokine*. **56**, 256–264 (2011).
46. Y. Kumamoto *et al.*, CD301b+ Dermal Dendritic Cells Drive T Helper 2 Cell-Mediated Immunity. *Immunity*. **39**, 1–11 (2013).
47. Bin Yang *et al.*, IL-27 Facilitates Skin Wound Healing through Induction of Epidermal Proliferation and Host Defense. *J. Invest. Dermatol.* **137**, 1166–1175 (2017).
48. M. S. Hu *et al.*, Delivery of monocyte lineage cells in a biomimetic scaffold enhances tissue repair. *JCI Insight*. **2** (2017), doi:10.1172/jci.insight.96260.
49. S. Werner, T. Krieg, H. Smola, Keratinocyte-fibroblast interactions in wound healing. *Journal of Investigative Dermatology*. **127**, 998–1008 (2007).
50. Y. Ando, P. J. Jensen, Epidermal Growth Factor and Insulin-Like Growth Factor I Enhance Keratinocyte Migration. *J. Invest. Dermatol.* **100**, 633–639 (1993).
51. I. Haase, R. Evans, R. Pofahl, F. M. Watt, Regulation of keratinocyte shape, migration and wound epithelialization by IGF-1- and EGF-dependent signalling pathways. *Journal of Cell Biology*. **116**, 3227–3238 (2003).
52. J. G. Simmons, J. B. Pucilowska, T. O. Keku, P. K. Lund, IGF-I and TGF-beta1 have distinct effects on phenotype and proliferation of intestinal fibroblasts. *Am J Physiol Gastrointest Liver Physiol*. **283**, G809–18 (2002).
53. S. M. Rudman, M. P. Philpott, G. A. Thomas, T. Kealey, The Role of IGF-I in Human Skin and its Appendages: Morphogen as Well as Mitogen? *J. Invest. Dermatol.* **109**, 770–777 (1997).
54. Y. Xin *et al.*, Expansion of CD26 positive fibroblast population promotes keloid progression. *Exp. Cell Res.* **356**, 104–113 (2017).
55. H. Suga *et al.*, Tracking the Elusive Fibrocyte: Identification and Characterization of Collagen-Producing Hematopoietic Lineage Cells During Murine Wound Healing. *STEM CELLS*. **32**, 1347–

1360 (2014).

56. B. Hinz, Formation and Function of the Myofibroblast during Tissue Repair. *Journal of Investigative Dermatology*. **127**, 526–537 (2007).
57. J. R. Rock *et al.*, Multiple stromal populations contribute to pulmonary fibrosis without evidence for epithelial to mesenchymal transition. *Proc Natl Acad Sci USA*. **108**, E1475–83 (2011).
58. K. M. Vannella, T. A. Wynn, Mechanisms of Organ Injury and Repair by Macrophages. *Annu. Rev. Physiol.* **79**, annurev–physiol–022516–034356 (2016).
59. D. G. Gilbertson *et al.*, Platelet-derived Growth Factor C (PDGF-C), a Novel Growth Factor That Binds to PDGF α and β Receptor. *J Biol Chem*. **276**, 27406–27414 (2001).
60. A. Triantafyllopoulou *et al.*, Proliferative lesions and metalloproteinase activity in murine lupus nephritis mediated by type I interferons and macrophages. *Proc Natl Acad Sci USA*. **107**, 3012–3017 (2010).
61. H. R. Chang, H. J. Kim, X. Xu, A. W. Ferrante Jr., Macrophage and adipocyte IGF1 maintain adipose tissue homeostasis during metabolic stresses. *Obesity*. **24**, 172–183 (2015).
62. P. Ramachandran *et al.*, Differential Ly-6C expression identifies the recruited macrophage phenotype, which orchestrates the regression of murine liver fibrosis. *Proc Natl Acad Sci USA*. **109**, E3186–95 (2012).
63. J. Tonkin *et al.*, Monocyte/Macrophage-derived IGF-1 Orchestrates Murine Skeletal Muscle Regeneration and Modulates Autocrine Polarization. *Mol Ther*. **23**, 1189–1200 (2015).
64. D. Pohlers, R. Huber, B. Ukena, R. W. Kinne, Expression of platelet-derived growth factors C and D in the synovial membrane of patients with rheumatoid arthritis and osteoarthritis. *Arthritis & Rheumatism*. **54**, 788–794 (2006).
65. S. E. Lynch, J. C. Nixon, R. B. Colvin, H. N. Antoniades, Role of platelet-derived growth factor in wound healing: synergistic effects with other growth factors. *Proc Natl Acad Sci USA*. **84**, 7696–7700 (1987).
66. S. E. Lynch, R. B. Colvin, H. N. Antoniades, Growth factors in wound healing. Single and synergistic effects on partial thickness porcine skin wounds. *Journal of Clinical Investigation*. **84**, 640–646 (1989).
67. S. E. Lynch *et al.*, The effects of short-term application of a combination of platelet-derived and insulin-like growth factors on periodontal wound healing. *J. Periodontol*. **62**, 458–467 (1991).
68. M.-I. Chung, M. Bujnis, C. E. Barkauskas, Y. Kobayashi, B. L. M. Hogan, Niche-mediated BMP/SMAD signaling regulates lung alveolar stem cell proliferation and differentiation. *Development*. **145**, dev163014–22 (2018).
69. P. C. Schwalie *et al.*, A stromal cell population that inhibits adipogenesis in mammalian fat depots. *Nature*, 1–28 (2018).
70. J. Conway *et al.*, Inhibition of colony-stimulating-factor-1 signaling in vivo with the orally bioavailable cFMS kinase inhibitor GW2580, 1–10 (2005).
71. S. J. Priceman *et al.*, Targeting distinct tumor-infiltrating myeloid cells by inhibiting CSF-1 receptor: combating tumor evasion of antiangiogenic therapy. *Blood*. **115**, 1461–1471 (2010).

72. E. Festa *et al.*, Adipocyte Lineage Cells Contribute to the Skin Stem Cell Niche to Drive Hair Cycling. *Cell*. **146**, 761–771 (2011).
73. B. A. Schmidt, V. Horsley, Intradermal adipocytes mediate fibroblast recruitment during skin wound healing. *Development*. **140**, 1517–1527 (2013).
74. A. M. B. Tadeu *et al.*, Transcriptional Profiling of Ectoderm Specification to Keratinocyte Fate in Human Embryonic Stem Cells. *PLoS ONE*. **10**, e0122493 (2015).
75. C. Trapnell *et al.*, Differential gene and transcript expression analysis of RNA-seq experiments with TopHat and Cufflinks. *Nat Protoc*. **7**, 562–578 (2012).
76. T. A. Wynn *et al.*, Quantitative assessment of macrophage functions in repair and fibrosis. *Curr Protoc Immunol*. **Chapter 14**, Unit14.22 (2011).
77. R. E. Mirza, M. M. Fang, W. J. Ennis, T. J. Koh, Blocking interleukin-1 β induces a healing-associated wound macrophage phenotype and improves healing in type 2 diabetes. *Diabetes*. **62**, 2579–2587 (2013).
78. H. M. McGee *et al.*, IL-22 Promotes Fibroblast-Mediated Wound Repair in the Skin. *Journal of Investigative Dermatology*. **133**, 1321–1329 (2012).